ACS OMEGA

http://pubs.acs.org/journal/acsodf

Article

FTIR Photoacoustic and ATR Spectroscopies of Soils with Aggregate Size Fractionation by Dry Sieving

Petr K. Krivoshein, Dmitry S. Volkov, Olga B. Rogova, and Mikhail A. Proskurnin*

Cite This: *ACS Omega* 2022, 7, 2177−2197

Read Online

ACCESS | Metrics & More | Article Recommendations | Supporting Information

ABSTRACT: Granulometric fractionation as a source of additional information on organic-matter and inorganic matrix components of soils using FTIR−photoacoustic spectroscopy (FTIR−PAS) supported by attenuated−total reflection FTIR spectroscopy (ATR−FTIR) for a wide range of aggregate fractions (10−5000 μm) was used to compare the sensitivity, reproducibility, information contents, and representativity of fractionated samples. For chernozem and sod-podzolic soils and different agricultural-use chernozem samples, differences in the composition were found, manifested in normalized spectra of microaggregate fractions, with the range of 10−100 μm bearing the complete information. Most changes are observed in the soil organic matter range (1900−1340 cm^{-1}), although these changes are slight, and in the soil-matrix region (550−300 cm^{-1}). The latter region increases the intensity of bands corresponding to amorphous silica and clay minerals in fine fractions, while the intensity of bands attributed to quartz lattice vibrations decreases. FTIR−PAS spectra do not differ considerably at high interferometer modulation frequencies as the signal-penetration depth is comparable with particle sizes. The soil fractions below 20 μm result in the maximum sensitivity, reproducibility, and signal-to-noise ratio, showing no changes from coarser fractions by the information content and, thus, providing representative samples for analysis. The fractionation shows more differences in the sod-podzolic and chernozem soil fractions than the whole soil spectra. FTIR−PAS provides better sensitivity and reproducibility in the 4000−2000 cm^{-1} region and ATR−FTIR in the 2000−100 cm^{-1} region.

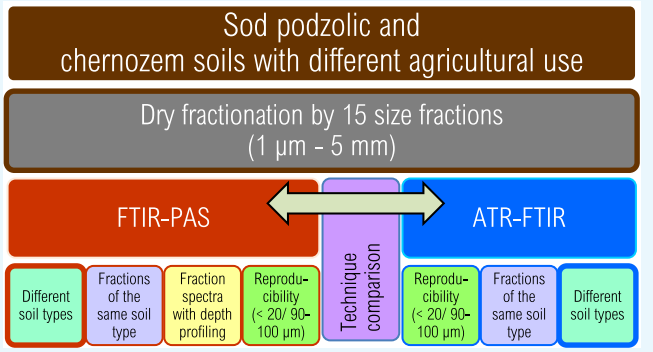

1. INTRODUCTION

There is an increasing need to study and monitor soils as the largest solid carbon reservoir,[1] identifying soil condition changes, including soil formation, degradation, remediation, environmental protection, and ecosystem integrity. Apart from bulk soil properties, studies on the roles of agricultural use and anthropogenesis on physical and physicochemical properties of soils become more topical.[2−4] A new and demanding challenge is characterizing the composition and structures of soil fractions, including changes at microaggregate levels.[5−9] The behavior of macroaggregates has been studied actively for a long time,[10−13] but the properties of microaggregates have been studied much less.[9] The critical problem of soil analysis is the characterization of soil organic matter (SOM) as an organomineral continuum of high- and low-molecular organic and inorganic substances in a finely dispersed state.[14,15]

Solving all these problems requires highly informative methods and approaches. Usually, the soil should be subjected to sample preparation for more detailed chemical analysis, including soil decomposition and the extraction of SOM individual components, which destroys the soil structure, and the results do not fully correspond to actual soil properties. Without distorting the soil and SOM composition, more information can be obtained with non-destructive molecular spectroscopy methods.[16,17]

Recently, the role of IR spectroscopy in soil and soil component studies has increased dramatically.[18−28] The most characteristic limits of detection of substances of different classes are 0.001−10% w/w with a relative standard deviation (RSD) of 0.05−0.20.[29,30] Despite its abilities, IR spectroscopy does not have the full resolution to provide complete information on the sample for soil characterization. Therefore, the data modeling should be used, or measurements should still be hyphenated with chemical or physical sample preparation. However, such pretreatment should minimally affect the soil. In IR spectroscopy, advantageous is the approach based on preparative fractionation (granulometric or densitometric).[16,17] In many aspects, it is an analogue of chromatography, which does not require transfer to the solution and almost does not change the

Received: October 12, 2021
Accepted: December 23, 2021
Published: January 4, 2022

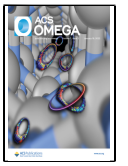

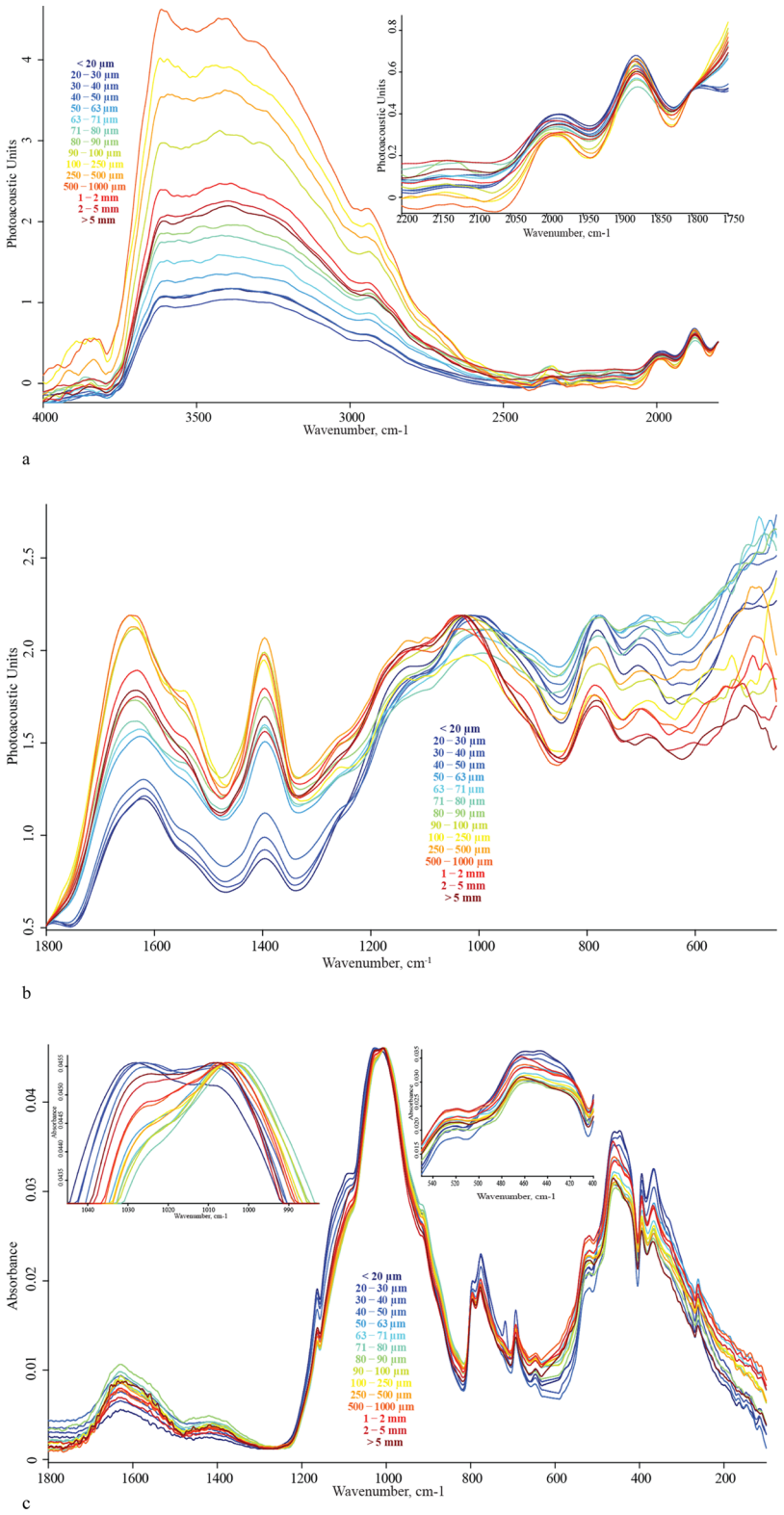

Figure 1. FTIR–PAS at an IMF of 1.6 kHz [(a) high wavenumber range and (b) low wavenumber range] and ATR–FTIR (c) spectra of native steppe chernozem soil fractions. Spectra are maximized by the band at 1007–1032 cm^{-1}. Regions of maximum changes are also presented as insets.

separated material chemistry. This approach is widely used in soil science; however, its combination with FTIR is not widespread.

FTIR–photoacoustic spectroscopy (FTIR–PAS), which appeared in a soil analysis two decades ago, now matured into a full-fledged characterization method[31−35] due to several advantages over other methods of IR spectroscopy of soils: a large number of well-defined bands and a broader range of the informational spectrum.[36−39] FTIR–PAS is an alternative to transmission, diffuse-reflectance, and attenuated–total reflection IR (ATR–FTIR) techniques and is less dependent on the particle size.[40] Recently, scatter PAS techniques in the frequency

https://doi.org/10.1021/acsomega.1c05702
ACS Omega 2022, 7, 2177−2197

Table 1. Band Assignments for Soils by FTIR−PAS and ATR−FTIR

band, cm^{-1}	inorganic (matrix) constituent	organic constituent	ATR	PAS
3730	Si−OH stretching (kaolinite, clay)	n/a	absent	shoulder
3700	Si−OH stretching, tilted (kaolinite, clay)	n/a	absent	medium
3670	hydrogen-bonded SiO−H H_2O stretch (amorphous)[55]	n/a	absent	weak
3620	Al(Mg)Si−OH stretching, straight	n/a	medium	intense
3600−2600	water, stretching, comprised of:	N−H stretching	medium	intense, broad
3490	asynchronous ν_3	O−H, phenolic, alcohol, carboxylic		
3270	synchronous, ν_1	O−H, phenolic, alcohol, carboxylic		
2940		C−H, CH_2 antisymmetric stretch[56−58]	weak	medium to weak
2860		C−H, CH_2 symmetric stretch	weak	medium to weak
1970	SiO_2 combination band ≅920 + 1037 or 970 + 1000[59]	C═O stretching	negative, artefact	medium
1880−1866	SiO_2 combination band ≅697 + 1163	C═O stretching	weak	intense
1783	SiO_2 combination band ≅697 + 1072	C═O stretching	weak	intense
1710−1680	SiO_2 combination band ≅760 + 920	N−H bending, amine Alkene−C═C−stretching	absent	weak shoulder
1650−1640	water, bending ν_2, absorbed	amide I, aromatic −C═C− stretching[60]	medium	intense, sharp
1620−1610	SiO_2 overtone ≅2 × 795	N−H bending, C═O stretching	medium, shoulder	intense
1460	SiO_2 amorphous combination band ≅ 350 + 1153	O−H, C−H scissoring	weak	shoulder
1410−1400	Mg−OH stretching[59]	C−O stretching	weak	medium
1250−1240	SiO_2 combination band ≅450 + 795	amide III, C−O stretch of aromatic rings and carboxylic acids,[61] C−O stretching, CH_2 rocking	absent	weak shoulder
1165	lattice SiO_2	n/a	medium	medium
1113	SiO_2	n/a	intense	intense
1095	SiO_2, silicate Si−O stretching[62]	in-plane C−H bending (non-aromatic) and cellulose (?)	intense	intense, shoulder
1070	lattice SiO_2, Si−O stretching (kaolinite, illite)[63]	n/a	intense	intense
1035−1020	silicate Si−O stretching (kaolinite, illite)	in-plane C−H bending (non-aromatic) and carbohydrates (?)	intense	intense, shoulder
1000	SiO_2, Si−O stretching lattice	n/a	intense	intense, shoulder
930−910	silicate, alumosilicate, overtone SiO_2 ≅2 × 450	n/a	intense	intense
860	Al−OH (clay minerals)	n/a	weak, shoulder	weak, shoulder
796	SiO_2, lattice stretching SiO_2 silicate[62]	out of plane (oop) C−H bending (non-aromatic)	intense	intense
697	SiO_2, Si−O−Si bending lattice	n/a	intense	intense
655	silicate, Si−O−Si bending, iron oxide	n/a	intense	medium
490	SiO_2, O−Si−O bending lattice	n/a	intense	shoulder
470	SiO_2, O−Si−O bending[62]	n/a	intense	intense
455−450	SiO_2, O−Si−O bending lattice	n/a	intense	intense
440	SiO_2, O−Si−O bending	n/a		
430−420	Mg−OH, Al−OH (clay minerals)	C−C in-phase vibrations[64]	intense	shoulder
400−395	SiO_2, O−Si−O bending lattice; water, librations	n/a	intense	intense
330	(?) Mg−O stretching[59]	n/a	medium, broad	medium, broad

regime have been proposed to study the morphology of aggregated samples and retrieve individual contributions of scattering and absorption of complex samples.[41,42] FTIR−PAS applications for soils are diverse: they involve matrix soil composition, the total SOM, the texture and mineralogy of clay minerals, the availability of nutrients, and the evaluation of other properties (fertility, structurization, and bacteriological activity).[38,43−46] Soil classification is carried out using principal component analysis, and the proportion of correctly identified samples in the control sample is usually more than 95%.[47,48] ATR−FTIR is also used for the organic matter content[49−51] and adsorbed water and minerals,[52] including nitrates.[47,53] Its advantages from the viewpoint of sample preparation and methodology are as follows: soil samples are pre-dried, the fraction of above 2 mm is usually sieved out, and the sample is placed on the crystal with a clamping screw. However, apart from changing the properties upon clamping, samples of dry soils may not provide good contact with the ATR crystal, which leads to a sensitivity loss and degraded precision of measurements. Simultaneously, wetting agents distort the results limiting this method.[54] Additional studies of all IR modalities are on-demand due to the soil complexity. ATR−FTIR and FTIR−PAS

https://doi.org/10.1021/acsomega.1c05702
ACS Omega 2022, 7, 2177−2197

are complementary to some extent, and their combined use is expedient from the viewpoint of qualitative and quantitative information.[39]

Thus, this study aimed to use aggregate fractionation as a source of additional information on soils using FTIR−PAS with ATR−FTIR as a second modality for a wide range of granulometric fractions (10−5000 μm) to identify the features of their composition and to compare the sensitivity, reproducibility, information content, and representativity of samples. This study selected dry-sieving fractionation as it provides no chemical changes and minimally affects the fraction composition upon separation. We used two soil types, sod-podzolic and typical chernozem, and for the latter, we compared samples with a significantly different agricultural use. The choice of these soils is due to the differences in the quantitative and qualitative composition of the organic matter caused by the contrast in the conditions of their formation: climatic, hydrological, lithological, vegetation cover, and microbiological activity. Thus, as a whole, the sample selection and separation method make it possible to assess the applicability of the accepted boundaries of particle size separation for the most reliable identification of differences in the composition of soils of different agricultural use from which such particles were isolated.

2. RESULTS

2.1. Band Identification and Fraction Comparison. To compare the possibilities of obtaining ATR-IR spectra of different fractions of chernozem and sod-podzolic soils, the IR spectra of the whole range of soil fractions were recorded, with purging the instrument and using a silicon broadband beam splitter (Figure 1). The regions 4000−3775 and 2560−2000 cm^{-1} contain many interfering bands of atmospheric water and carbon dioxide and artifacts associated with the ATR−FTIR diamond crystal absorption and are excluded from the analysis. The spectra were smoothed over 25 points; however, after this procedure, significant noise is still observed at 4000−1700 cm^{-1}, and the intensities of the characteristic bands are low. In this range, the ATR radiation penetration depth, eq 2, does not exceed 1.6 μm, and this range was also excluded. Thus, we considered the following regions: hydrogen-bond region (3775−3100 cm^{-1}), CH region (3100−2560 cm^{-1}), SOM region (2000−1340 cm^{-1}), matrix II (quartz/silica overtone, 1340−800 cm^{-1}), and matrix I (quartz lattice, 840−200 cm^{-1}). These regions were selected to contain a dominating type of bands and can be readily selected in the same manner for all the similar samples; some boundaries (e.g., 1340 or 1260 and 1900 or 1780 cm^{-1}) may be provisional but still reliable.[39] The bands are summed up in Table 1; the band integration results are presented in Tables S1−S5 (Supporting Information).

2.1.1. Hydrogen-Bond Region (3775−3100 cm^{-1}). The most intense bands in this region are O−H stretching vibrations with a broad continuum at 3500−3000 cm^{-1} corresponding to O−H and N−H vibrations of water, inorganic as well as organic fragments (alcohols, phenols, and amides)[56−58] linked by hydrogen bonds. The band with a maximum at 3730 cm^{-1} is assigned to the stretching vibrations of isolated non-sorbed water and stretching Si−O−H vibrations of hydrosilicates.[32,56,65] The band at 3695 cm^{-1} is related to stretching SiO−H vibrations, presumably belonging to kaolinite, and at 3620 cm^{-1}, to labile SiO−H vibrations of quartz and (mixed-layer) aluminosilicates.[55]

The band at 3730 cm^{-1} is manifested in all spectra of chernozem soil of native-steppe, cropland, and bare-fallow types with a particle size of <20, 20−30, and 50−63 μm and in shelterbelt of <20, 20−30, 50−63, 63−71, 80−90, and 100−250 μm. After vector normalization, a blue shift of the band maximum is observed with particle size. In sod-podzolic soil, this band manifests itself as a shoulder for fractions of 20−30 and 100−250 μm.

The band at 3695 cm^{-1} is present in all the samples and has the lowest intensity for bare-fallow fractions of 1−2, 2−5, and >5 mm and native steppe and cropland fractions >5 mm. On the contrary, for shelterbelt, this band has the lowest relative intensity for fine fractions of <20 and 20−30 μm. In sod-podzolic soil, the integral area of this band is in the range of 0.005−0.014 abs. units and increases with the particle size. The band shape and the maximum position are reproduced for all fractions, except for the chernozem cropland of 20−30 μm.

The band at 3620 cm^{-1} is not manifested in bare-fallow and native-steppe chernozems and is less expressed in shelterbelt and cropland fractions of <20, 20−30, and 80−90 μm, respectively, which is confirmed by the integral area of this band. This band has the highest intensities for coarse sod-podzolic fractions (500−1000 μm, 1−2 mm, and >5 mm); the integral area, similarly to 3693 cm^{-1}, increases with particle size. The satisfactory reproducibility of the band-maximum position is shown in all the cases.

2.1.2. CH Region (3100−2560 cm^{-1}). This region contains stretching vibrations $-CH_x$; the assigned bands are asymmetric 2920 cm^{-1} and symmetric 2860 cm^{-1} vibrations attributed to sp^3 $-CH_2$.[59,63] In bare fallow, only for particle sizes <20, 20−30, and 250−500 μm, it is possible to obtain non-negative integrals of both bands. These bands are the most intense for cropland for a fraction of 500−1000 μm; only for fractions of 20−30 and 250−500 μm, non-negative area integrals of both bands were obtained. The symmetric band of 2860 cm^{-1} is better manifested in native steppe fractions, though these bands could not be distinguished in fractions of 2−5 μm and 2−5 mm. In the shelterbelt, the 2860 cm^{-1} band appears in all the spectra and has non-zero integral areas, while the band at 2920 cm^{-1} is absent in most spectra and has the highest integral area in the largest fraction of >5 mm. After vector normalization, these bands do not become more pronounced. In all the chernozem soils, the actual maximum positions of both bands vary within 10 cm^{-1}. A low-intensity shoulder band at 2950 cm^{-1} appears, attributed to CH_3 groups.

In contrast to chernozems, in sod-podzolic soil, both 2920 and 2860 cm^{-1} bands are more pronounced and manifested in all spectra, and the maxima are flatter than the sharp maxima in chernozems. The integral areas of both bands increase with the particle size; the largest is for a fraction of 500−1000 μm. In this region, sod-podzolic soil also shows the broad band at 2670−2600 cm^{-1}, probably caused by the stretching N−H vibrations; its intensity does not depend on the fraction size. This region has a significant absorption for chernozem fractions of <20, 20−30, and 50−63 μm.

2.1.3. SOM Region (2000−1340 cm^{-1}). This region is the most difficult from the viewpoint of assessment, as it contains many bands attributed to SOM and overtone and combination bands of the soil matrix. The triplet of 1980, 1860, and 1780 cm^{-1} is a quartz matrix signature.[38,59] However, the band at 1860 cm^{-1} may belong to humic and other organic compounds (−C═O stretching vibrations[66,67]), and the band at 1785 cm^{-1} may be attributed to −C═O stretching vibrations.[68] Apart from the water band at 1640−1620 cm^{-1}, the broad band at 1750−1500 cm^{-1} contains stretching vibrations of carbonyl, bending

https://doi.org/10.1021/acsomega.1c05702
ACS Omega 2022, 7, 2177−2197

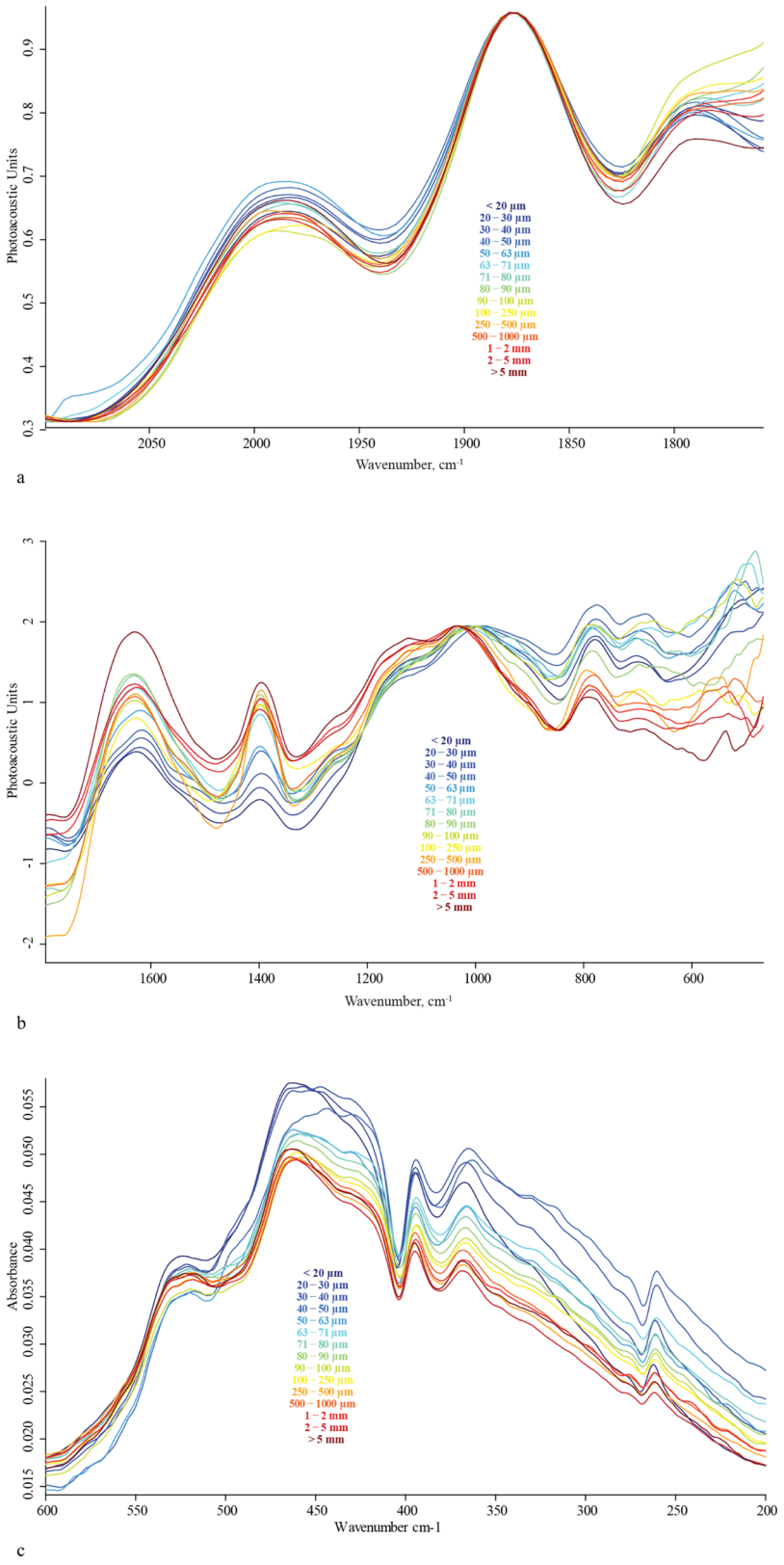

Figure 2. FTIR–PAS spectra at an IMF of 1.6 kHz [(a) high wavenumber range and (b) low wavenumber range] and (c) ATR–FTIR spectra of cropland chernozem soil fractions; the region of maximum changes in the fraction spectra.

deformation $-NH_2$ at 1680 cm^{-1}, stretching $-C{=}C-$ vibrations, and stretching $-C{=}O$ vibrations[56−58] as well as combination quartz bands at 1710−1680 and 1620−1610 cm^{-1}. The band at 1620 cm^{-1} is also referred to stretching C=O vibrations and bending amine vibrations.[68] The broad band at 1470−1345 cm^{-1} can be attributed to the quartz combination bands.[69,70] The bands at 1860 and 1785 cm^{-1} are absent in bare-fallow, shelterbelt, and cropland chernozem fractions, barely

https://doi.org/10.1021/acsomega.1c05702
ACS Omega 2022, 7, 2177−2197

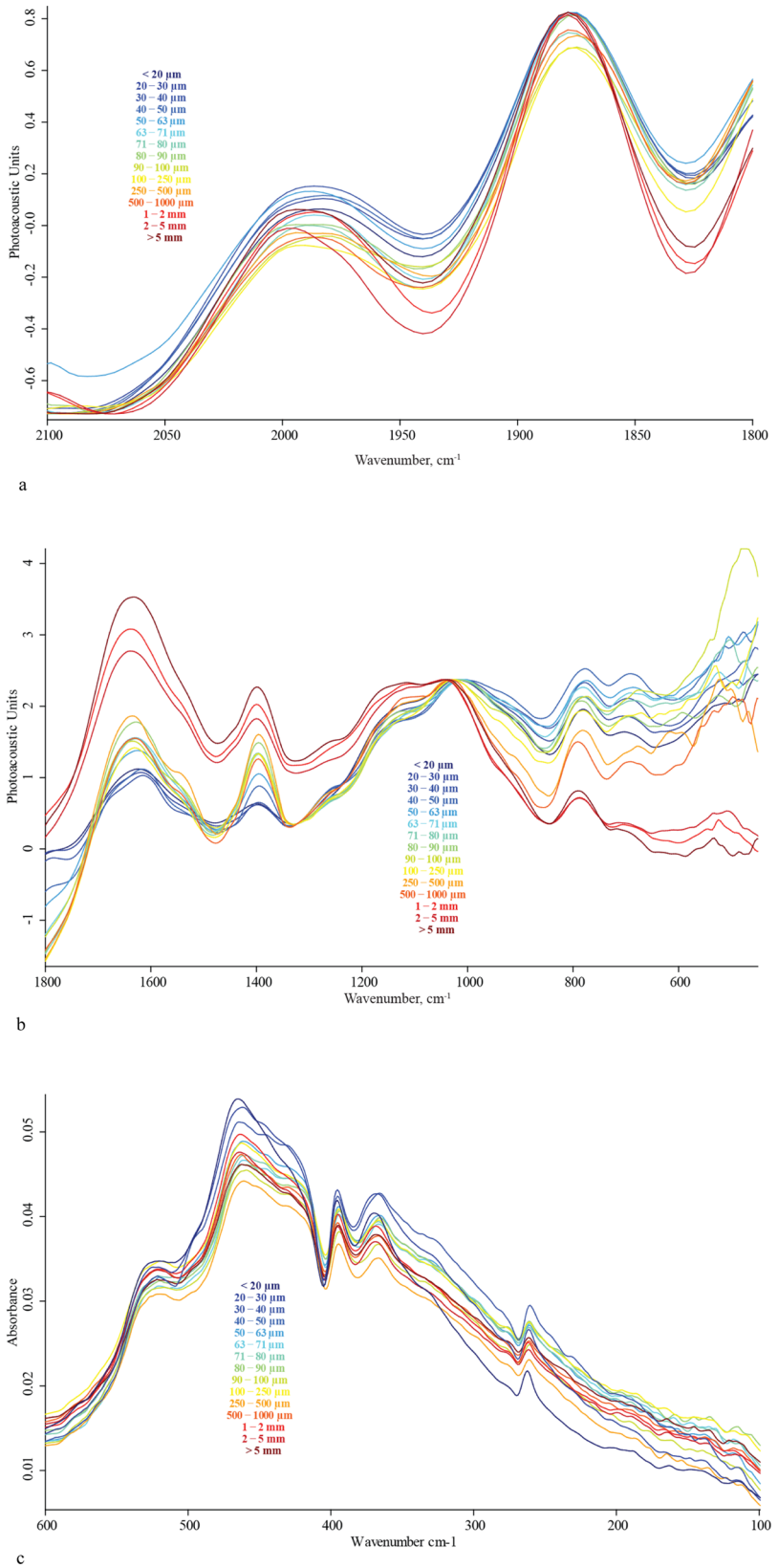

Figure 3. FTIR–PAS spectra at an IMF of 1.6 kHz [(a) high wavenumber range and (b) low wavenumber range] and (c) ATR–FTIR spectra of shelterbelt chernozem soil fractions; the region of maximum changes in the fraction spectra.

visible in native-steppe spectra but more pronounced in the spectra of the sod-podzolic soil. All other bands are present in all the fractions of all the samples.

For chernozem soils, the largest areas of these bands have fractions of the bare fallow, native steppe of <20 μm, as well as 1–2 and 2–5 mm. The largest band areas in this region for

https://doi.org/10.1021/acsomega.1c05702
ACS Omega 2022, 7, 2177–2197

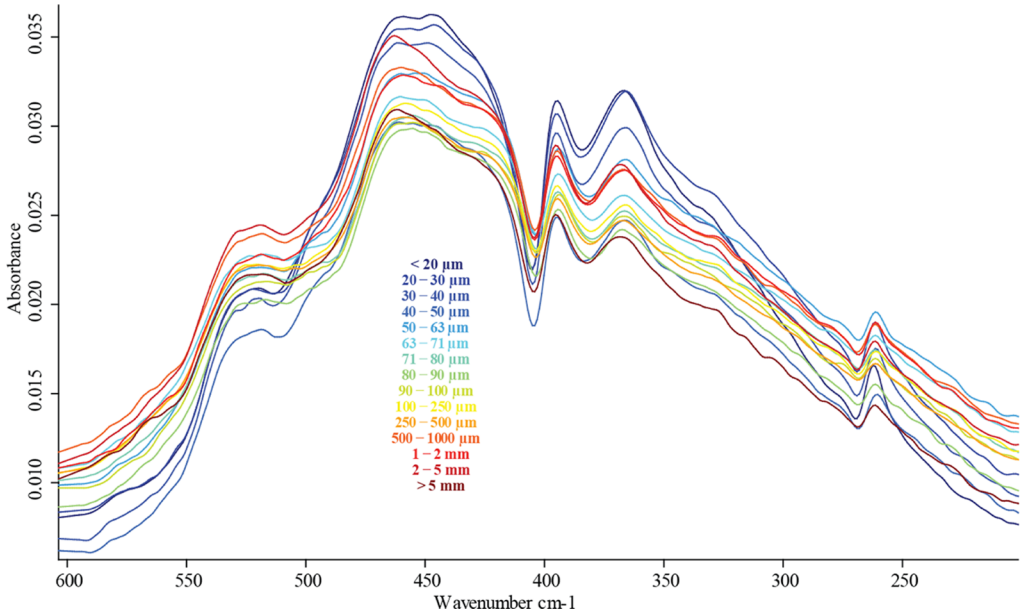

Figure 4. ATR−FTIR spectra of native steppe chernozem soil fractions; the region of maximum changes in the fraction spectra.

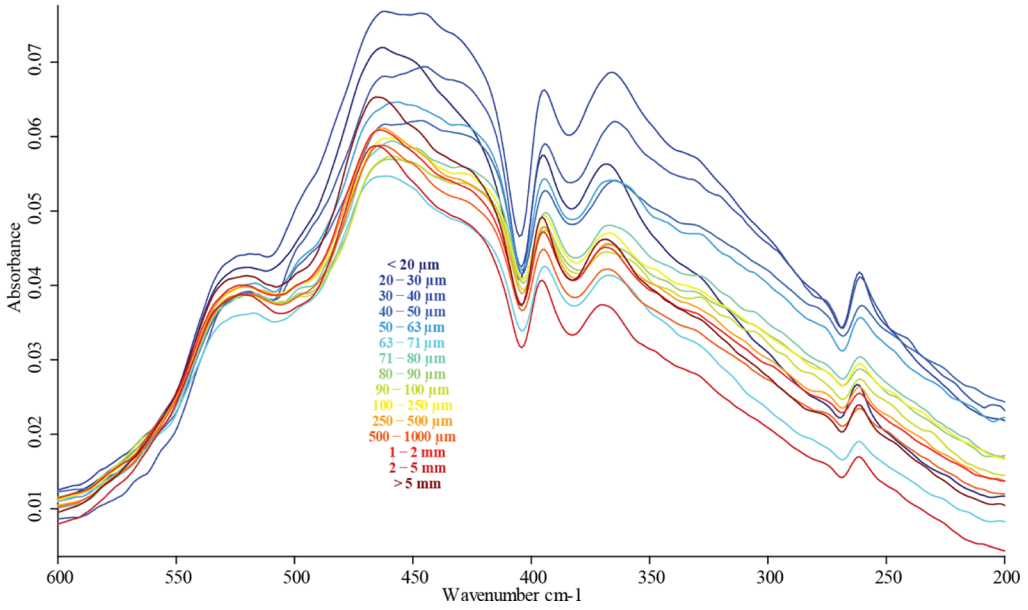

Figure 5. ATR−FTIR spectra of bare fallow chernozem soil fractions; the region of maximum changes in the fraction spectra.

shelterbelt are for coarse fractions of 1−2 and >5 mm. For the native steppe, the smallest band areas at 1620 cm^{-1} are observed for the fine fractions of <20 and 20−30 μm. In chernozems, intensities increase with the particle size; in sod-podzolic soil, the smallest band areas are for the fractions of 50−63 and 80−90 μm.

The positions of the maxima and the shape of bands are reproduced for all samples except for the sod-podzolic soil spectrum with a particle size of 2−5 mm: there is a different ratio of band intensities and, as a result, the spectrum has different intensities after vector normalization. The band at 1405 cm^{-1} has a shape different from others in the spectra of fine fractions of <20, 20−30 μm for bare fallow, native steppe, and cropland: these bands have a slightly sharper peak shifted to longer wavelengths.

A small band at 1740 cm^{-1} is also present in the sod-podzolic soil, attributed to the quartz matrix and the stretching −C═O vibrations.[68] Also, the band at 1550−1540 cm^{-1}, which can be attributed to bending amide −NH− vibrations,[68] appears in this spectrum of the sod-podzolic soil, but not chernozems.

2.1.4. Matrix II Region (1340−800 cm^{-1}). This region contains mainly bands of the soil matrix: quartz or hydrosilicates. A broad band includes a group of overlapped bands: 1250−1240 cm^{-1} corresponds to C−O stretching vibrations in phenol or−O−C═O in carboxylic acids.[71] In the region of 1190−900 cm^{-1}, several O−Si−O bands in quartz (prominent are 1165, 1111, 1095, 1037, 1020, and 1000 cm^{-1}) overlap. The shoulder with a maximum at 915 cm^{-1} corresponds to bending Al/Mg−O−H vibrations.[57] The 860 cm^{-1} band corresponds to bending Al−O−H vibrations.

https://doi.org/10.1021/acsomega.1c05702
ACS Omega 2022, 7, 2177−2197

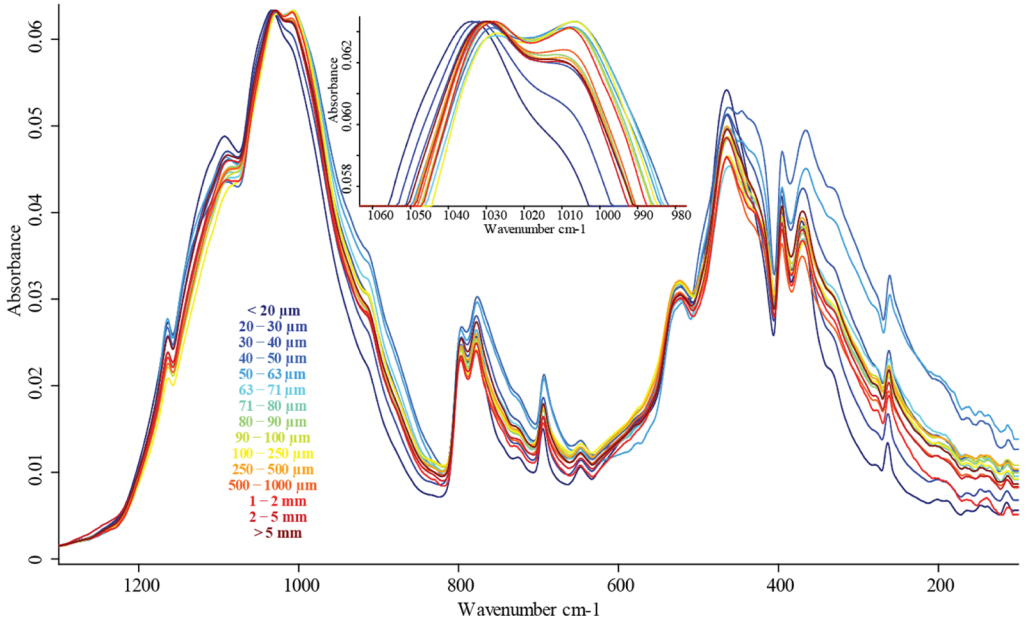

Figure 6. ATR−FTIR spectra of fractions of sod-podzolic soil. Regions of maximum changes are also presented as an inset.

All the bands in this region in chernozem tend to decrease with the fraction size, but a new increase in integral areas is observed from the fraction of 250 μm onward. The same regularity is found for bands at 1190−900 cm^{-1}: fine fractions <20 and 20−30 μm have the largest integrals. The spectra of coarse fractions of 2−5 and >5 mm have a different baseline and, therefore, different band intensities after vector normalization. The integrals of these bands are comparable to those of the smallest fractions. Furthermore, for the shoulder at 990 cm^{-1} (Si−O stretch), an almost uniform increase in band areas is observed with the particle size. In addition to these bands of quartz, the spectra of sod-podzolic soil show a band at 1260 cm^{-1}, which corresponds to both the quartz matrix and possible bending vibrations of carboxyl or amide (amide III). For native steppe chernozem fractions of <20 and 20−30 μm, a redshift of the maxima is observed for all bands with varying soil particle sizes, whereas no shift is found for shelterbelt and cropland.

2.1.5. Matrix I Region (840−200 cm^{-1}). As the matrix II region, this region also predominantly contains the most intense lattice bands of the quartz matrix (796, 775, 697, 490, and 450 cm^{-1}), Figures 2−6. In the region of 640−610 cm^{-1}, libration bands of the atmospheric water are manifested. The 775 cm^{-1} band belongs to the deformation vibrations of Al/Mg−O−H[57] or quartz.[63,72]

The lattice quartz bands appear in all spectra; bands at 775 and 697 cm^{-1} have a blueshift of the maxima for coarser fractions. These bands have the highest intensities in the spectra of samples with particle sizes <20 and 20−30 μm. Sod-podzolic soil shows the best reproducibility. All the above bands have the same shape for all the fractions. With an increase in the size, there is a slight redshift by 2−3 cm^{-1}. In the fine fractions of <20 and 20−30 μm, a shoulder at 490 cm^{-1}, Si−O−Si deformation, appears. All the soil-type fractions of 100−250 μm and 2−5 mm have additional bands at 720 and 670 cm^{-1}. The bands at 670−400 cm^{-1} are not reproduced from spectrum to spectrum.

2.2. Signal Penetration Depth. The penetration depth of radiation in the soil in ATR−FTIR was estimated using eq 2 with a refractive index of the sample as quartz n_S = 1.54 and the refractive index of the diamond ATR crystal as n_{ATR} = 2.418 (Figure S1a; Supporting Information). To estimate the penetration depth of radiation by FTIR−PAS, we performed a model calculation for interferometer modulation frequencies (IMFs) of 1.6−10 kHz using eq 1. D_T of 50 cm^2/h (1.4 × 10^{-6} m^2/s) for soil[73] and 4.5 × 10^{-6} m^2/s for quartz[74] were used.

The penetration depth of radiation for FTIR−PAS in all the mid-IR region is 35−100 μm at IMF of 1.6 kHz (Figure S1b; Supporting Information), which is comparable with the size of fine and medium fractions, while the penetration depth for the ATR−FTIR modality is 1−8 μm, which is below the particle size of all the fractions and significantly inferior to FTIR−PAS. Only at 200−100 cm^{-1}, the ATR−FTIR penetration depth becomes 10−20 μm and thus comparable with the particle size of the finest fraction and the penetration depth in FTIR−PAS.

Thus, the choice of fractions for further comparison is primarily due to the radiation penetration depth: for interferometer modulation frequencies of 1.6 and 2.5 kHz, the maximum value in FTIR−PAS, at 400 cm^{-1} are ca. 100 and ca. 85 μm, respectively; for 7.5 and 10.0 kHz, ca. 50 and ca. 40 μm, respectively. Thus, the fractions below 100 μm are almost wholly smaller than the radiation penetration depth. Furthermore, for the ATR−FTIR variant, the maximum radiation penetration depth of 25 μm reached for the wavenumber of 100 cm^{-1}. This depth corresponds to a fraction of <20 μm. Therefore, while in ATR−FTIR, all the measurements correspond to a single layer of soil particles at contact with the crystal; in FTIR−PAS, the radiation for fine fractions passes completely through several particles, and each particle emits thermal waves in all directions of space.[75]

2.3. Reproducibility of Spectral Information. To test and compare the reproducibility of measurements, we used fractions of <20 μm as well as 90−100 μm as providing similar conditions for both methods (particle size is larger than the penetration depth). The medium fraction was also selected as it is not tiny enough to be decomposed with the clamping screw at ATR−FTIR measurements. Shelterbelt chernozem soil was selected as giving medium intensities of the characteristic bands. Ten replicate spectra (Figure S2, Supporting Information) were recorded with complete replacement of the sample in the sample

https://doi.org/10.1021/acsomega.1c05702
ACS Omega 2022, 7, 2177−2197

cup (FTIR−PAS) or crystal (ATR−FTIR) with vector normalization of the spectra and calculating RSD of the obtained integral areas of all the assigned bands using eq 3. The dependences of the RSD on wavenumber are shown in Figure S3, Supporting Information; Tables 2−4 show the band integrals and RSD values for FTIR−PAS and ATR−FTIR spectra. The calculation and comparison of the averaged signal-to-noise for the significant bands were performed, as shown in Figure S4, Supporting Information.

Table 2. Reproducibility of ATR−FTIR for Main Characteristic Bands for the Soil Fraction of Below 20 μm

band center, cm^{-1}	high-wave boundary, cm^{-1}	low-wave boundary, cm^{-1}	RSD
3744	3761	3727	4.24
3700	3717	3683	0.15
3620	3637	3603	0.17
3590	3600	3581	2.60
2920	2942	2903	0.76
2850	2868	2839	1.06
2629	2668	2589	0.22
1879	1921	1837	0.13
1798	1814	1782	0.19
1653	1662	1644	0.50
1608	1629	1587	0.18
1430	1455	1404	0.06
1175	1193	1157	0.05
998	1067	930	0.06
909	926	893	0.07
780	819	741	0.05
687	706	669	0.06
641	656	625	0.04
529	544	513	0.05
441	478	405	0.08
393	403	384	0.11
362	371	354	0.56

Low IMFs significantly increase the recording time in FTIR−PAS, up to 30 min. Thus, to balance the recording time and a minimum deterioration in the signal-to-noise ratio, we have selected the IMF of 1.6 kHz; this makes it possible to achieve a radiation penetration depth of up to 100 μm, and the spectrum registration time is ca. 5 min.

2.3.1. Fraction <20 μm. For the finest fraction <20 μm, low-intensity bands belonging to the OH vibrations of environmental water do not exceed the noise signal at 4000−3775 cm^{-1} (Figure S4, Supporting Information). At 3775−3000 cm^{-1}, the reproducibility of bands at 3690 and 3620 cm^{-1} show RSD values of 0.15 and 0.17, respectively. Weak bands at 3740 and 3600 cm^{-1} have the worst RSDs. From the viewpoint of the band-maximum position, high-intensity bands at 3690 and 3620 cm^{-1} are reproducible, and the 3620 cm^{-1} band has a worse band shape reproducibility.

In the CH region (3100−2560 cm^{-1}), the band at 2920 cm^{-1} is more reproducible than 2860 cm^{-1} (Tables 2 and 3). The band width of 2920 cm^{-1} and its maximum position can vary within 10 cm^{-1}. The band at 2670−2630 cm^{-1} is reproduced better than other bands in this region. A severe increase in RSD is observed at 2350−2200 cm^{-1} due to the atmospheric CO_2 band; the region of 2200−1900 cm^{-1} is dominated by the characteristic band of sp^3 C−C of the diamond ATR crystal.

Table 3. Reproducibility of FTIR−PAS for Main Characteristic Bands for the Soil Fraction of Below 20 μm

band center, cm^{-1}	high-wave boundary, cm^{-1}	low-wave boundary, cm^{-1}	RSD
3744	3760	3727	0.122
3700	3717	3683	0.114
3670	3677	3663	0.218
3652	3663	3640	0.115
3620	3636	3602	0.142
3590	3600	3580	0.696
2919	2942	2896	0.187
2840	2875	2838	0.178
2166	2175.9	2155.86	4.320
2140	2156.5	2124.38	1.794
1980	2050.6	1955.83	0.128
1942	1949.79	1934.5	0.394
1860	1920.85	1836.9	0.114
1808	1833.08	1782.2	0.200
1772	1779.65	1763.75	0.070
1735	1742	1727	0.086
1652	1662	1642	0.083
1620	1628	1587	0.312
1559	1566	1550	0.587
1539	1547	1530	0.116
1523	1529	1515	0.583
1484	1742	1225	0.382
1364	1662	1066	0.379
1277	1628	925	0.282
780	818	740	0.082
697	718	676	0.103
641	655	625	0.652
523	533	513	1.541

Table 4. Reproducibility of ATR−FTIR for Main Characteristic Bands for the Soil Fraction of 90−100 μm

band center, cm^{-1}	high-wave boundary, cm^{-1}	low-wave boundary, cm^{-1}	RSD
3744	3761	3727	1.01
3670	3717	3683	0.30
3620	3637	3603	0.30
3590	3600	3581	1.06
2923	2942	2903	0.84
2860	2868	2839	0.77
2629	2668	2589	0.20
1879	1921	1837	0.482
1798	1814	1782	0.375
1653	1662	1644	0.84
1608	1629	1587	0.65
1430	1455	1404	0.29
1175	1193	1157	0.14
998	1067	930	0.21
909	926	893	0.22
780	819	741	0.19
687	706	669	0.19
641	656	625	0.17
529	544	513	0.18
441	478	405	0.19
393	403	384	0.20
362	371	354	0.77

In the SOM region (1900−1340 cm^{-1}), the bands at 1880 and 1798 cm^{-1} have satisfactory reproducibility: the widths and

https://doi.org/10.1021/acsomega.1c05702
ACS Omega 2022, 7, 2177−2197

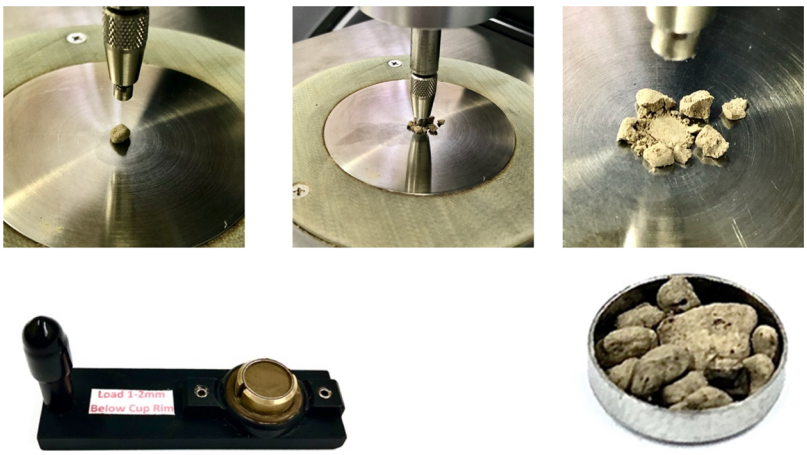

Figure 7. Upper part: the process of forming a compressed disk when recording an IR spectrum of a soil aggregate with a particle size of 2−5 mm on an ATR attachment; lower part: the view of the FTIR−PAS holder with a cup filled with a fine fraction of the soil and an example of filling a 10 mm i.d. cup with a soil fraction of 2−5 mm. Photograph courtesy of P.K.K.

maximum positions of these bands are stable. All bands overlap at their base in 1760−1460 cm^{-1}; still, band maxima and half-widths show satisfactory reproducibility (Table 3).

In matrix I and II regions, there is an insignificant difference in the baseline height, but the RSD of band integrals in the matrix II region does not exceed 0.07; all bands are reproduced both in shape and in maximum positions (Table 2). In the region of 840−400 cm^{-1}, all the bands have an RSD exceeding 0.1 (Table 2), a change in the baseline intensity in the region of 500−350 cm^{-1} is observed, but these differences insignificantly affect band reproducibility. As mentioned above, above 400 cm^{-1}, excellent band reproducibility is observed for integral areas, maximum positions, and band shapes. Below 400 cm^{-1}, differences are observed in the maximum positions of low-intensity bands. Thus, there is a general improvement in band reproducibility with decreasing wavenumbers.

2.3.2. Fraction 90−100 μm. For a fraction of 90−100 μm (Table 4 and Figure S4, Supporting Information) after the vector normalization procedure, the signal-to-noise ratio for the band at 3690 cm^{-1} increases. In the hydrogen-bond region (3775−3100 cm^{-1}), RSD values for the band integrals are higher than the fine fraction of <20 μm. For the most intense bands at 3670 and 3620 cm^{-1}, a deterioration in RSD of the integration results is observed with an increase in the particle size. For the rest, RSD exceeds 1.0 despite the normalization procedure. In this region, only one band has an unchanged position of the maximum, 3670 cm^{-1}. In other cases, a shift of the maxima is observed and low reproducibility of the band shape. In the CH region (3100−2560 cm^{-1}), compared to <20 μm, bands at 2920 and 2860 cm^{-1} have lower reproducibility in shape and maximum position. CH_2 bands have an RSD not exceeding 0.5; thus, an increase by more than 0.2 is observed. In the SOM region (1900−1340 cm^{-1}), with an increase in the particle size, an increase in the RSD values for the obtained band integrals is observed (Table 4). RSD barely exceeds 0.2 for all the bands identified in the matrix II region. Compared with the results obtained for soil with particle sizes <20 μm, the RSD of band integrals increased by 0.07−0.14. In the matrix I region, RSD does not exceed 0.2. As the fine fraction of <20 μm, up to 400 cm^{-1}, excellent band reproducibility is observed in terms of integrals, positions of maxima, and band shape. Below 400 cm^{-1}, differences are observed in the positions of the maxima of the low-intensity bands.

In both fractions, a general improvement in the reproducibility of spectral absorption bands is observed for the longwave subrange. The fine fraction of <20 μm has better reproducibility in comparison with the medium fraction of 90−100 μm: in the regions 3500−2350 and 1200−400 cm^{-1} RSD, it was 0.06−0.12; for particles with a size of 90−100 μm in these regions, the RSD values were 0.14−0.31. The method allows obtaining results with an error of ±0.001 absorption units (8.5% of the average value) to ±0.0045 units (4.5% of the average value) for the OH region of 4000−2500 cm^{-1} and the fingerprint region of 1200−400 cm^{-1} for soils with a particle size <20 μm. Moreover, for a fraction of 90−100 μm, ATR−FTIR spectra recording is possible with an error of ±0.003 absorption units (15% of the average absorption value) to ±0.01 conventional absorption units (14% of the average value) for the OH region and the fingerprint region, respectively.

3. DISCUSSION

3.1. Comparison of Soil Fractions. In most ATR−FTIR spectra of soil fractions, a similar pattern is observed for all the samples: for smaller fractions, there is a decrease in the intensities and integrals of the bands with an increase in the fraction size but starting from fractions of 250−500 or 500−1000 μm, the integral areas begin to increase again, so in some cases, the band areas for soil fractions larger than 5 mm exceeded those for fractions smaller than 20 μm. However, the intensity ratio is different from similar studies. For example, for chernozems of the bare fallow type in the region 1200−100 cm^{-1}; according to Udvardi et al.[76] an exponential increase in characteristic band intensities should be traced with a decrease in the particle size. However, though the particle sizes of smaller fractions are comparable with the sizes in the study by Udvardi et al.,[76] we did not obtain a similar dependence (Figures 2−6): the smallest fraction has the highest intensity, after which intensities decrease, and samples with particle sizes from 100 μm to 5 mm are in random order. Thus, we have a different trend compared to the study by Cantero-Tubilla and Walker[77] In this work, particles of <20 μm were obtained exclusively by dry sieving, while these authors resorted to grinding particles with a size of 0.5 mm to only 75 μm; thus, the results may be partially distorted by possible mechanochemical transformations.[77] In our case, the reason for a random change in the band intensities of large soil fractions can be the uncontrolled destruction of soil

https://doi.org/10.1021/acsomega.1c05702
ACS Omega 2022, 7, 2177−2197

aggregates upon sample fastening with an ATR−FTIR clamping screw (Figure 7), while samples up to 100 μm in size are evenly fixed with the screw without visible destruction of soil aggregates, and even for a slight pressure, the pressed aggregates from a good contact with the crystal. Larger particles are readily destroyed by pressure in an uncontrolled manner to smaller particles forming a compressed disk. This could increase the intensities of nominally large fractions.

Apart from changes in the intensities of separate bands, there are changes in the relative intensities of neighboring bands, especially at 1050−980 cm^{-1} (Figure 1, insets and Figure 6, inset). In our opinion, this relates to the changes in the form of the SiO_2 matrix: while in the larger fractions, both FTIR−PAS and ATR−FTIR show the higher intensity of the band at 1000 cm^{-1} corresponding to the lattice vibrations of the crystalline quartz; finer fractions show a more intense band at 1030 cm^{-1} corresponding to amorphous silica and clay minerals. It is worth mentioning that although the spectra of chernozem and sod-podzolic soil are relatively similar, fractionation shows much more distinct changes of this region between the two types of soil. While all the chernozem fractions show comparable intensities of bands at 1030 and 1000 cm^{-1}, fine fractions of sod-podzolic soil show almost no intensity at 1000 cm^{-1}, which may be accounted for relatively low contents of crystalline quartz species in these fractions.

A similar picture is observed in the region 550−400 cm^{-1}. A decrease in the fraction size results in the increase in intensities at 490 and 470 cm^{-1} as well as 455 and 440 cm^{-1}, which are attributed to SiO_2 bending O−Si−O vibrations.[63] Higher wavenumbers correspond to amorphous species in these band pairs, while lower to quartz.[62,63] For these two band pairs, sod-podzolic soil shows higher contents of amorphous species in all the fractions (also, the two finest fractions show mostly amorphous species), while chernozems show much higher intensities of bands attributed to lattice vibrations, with fine fractions showing higher intensities of amorphous species.

Finally, significant differences in spectra are shown for 350−300 cm^{-1}, which have a wide band centered at 330 cm^{-1} attributed to Mg−O stretching.[59] Sod-podzolic soil and chernozems of all agricultural-use types differ by this band intensity (Figures 1 and 6), while chernozems show relatively high intensities of this band only for fine fractions. This band can also be used for differences in spectra of chernozem types. Native steppe and shelterbelt show high intensities of this band only for fractions of <20 and 20−30 μm, but bare fallow and cropland spectra of five fine fractions up to 50−63 μm show intense absorption of this band and are different from coarser fractions.

In our opinion, these results are somewhat relevant for soil analysis; the existing data for this region are relatively scarce, and the attribution of the bands at 500−300 cm^{-1} solely to quartz, silica, or clay minerals is somewhat ambiguous; thus, it requires further studies, probably with model samples of various mineral matrices to further clarify the nature of these changes.

Summing up the spectral changes for the whole studies fraction range, it can be stated that native steppe (Figures 1 and 4) and shelterbelt (Figure 3) chernozem samples show fewer differences in fractions compared to cropland and bare fallow (Figures 2 and 5, respectively). It manifests a more diverse composition and structuration of soil aggregates of different sizes in the latter two agricultural-use types. Thus, dry-sieving fractionation did not result in additional bands among the fractions; however, despite the scatter of intensities of coarse soil fractions, most characteristic bands with good intensity indicators are observed in the spectra of the finest soil fractions <20 μm.

A comparison of ATR−IR spectra of different chernozem soils reveals the similarity of three types: bare fallow, cropland, and shelterbelt, but the latter has more intense quartz bands of 1095, 1020, and 1000 cm^{-1}. The total intensity of the native steppe spectrum is somewhat lower in the regions of intense absorption of stretching 1160−800 cm^{-1} and bending vibrations of 700−300 cm^{-1} of quartz and silica. However, in the region of deformation non-aromatic −C−H vibrations of 796 cm^{-1} and deformation vibrations of clay materials (Al−O−H or Mg−O−H), the difference in the intensities for chernozems is also minor. The spectra of the sod-podzolic soil also have a lower intensity.

3.2. Reproducibility of IR Techniques. For both ATR−FTIR and PAS−FTIR for two fractions of the same soil type, the RSD of the band integrals increases with the particle size (Figure S3, Supporting Information). However, the decrease in the signal-to-noise ratio depends on the region. At 4000−3775 cm^{-1}, the signal-to-noise ratio deteriorates from 20 to 80% for FTIR−PAS and 40 to 60% for ATR−FTIR. At 3775−3000 cm^{-1}, the similar values are from 60 to 80% for FTIR−PAS and from 40 to 140% for ATR−FTIR. At 3000−2560 cm^{-1}, the signal-to-noise ratio deterioration is from 60 to 120% for FTIR−PAS and from 80 to 85% for ATR−FTIR. In the SOM region of 2060−1340 cm^{-1}, the signal-to-noise ratio deteriorates from 20 to 90% for FTIR−PAS and from 70 to 105% for ATR−FTIR. In the region of 1340−400 cm^{-1}, the signal-to-noise ratio deteriorates from 45 to 85% for FTIR−PAS and from 25 to 125% for ATR−FTIR.

In FTIR−PAS, the signal-to-noise ratio for soil fractions differing from each other by a factor of five worsens the signal-to-noise ratio by no more than 50%; but the absolute noise increase corresponds to the regions pf 3000−2560 and 1350−400 cm^{-1}. Comparing the reproducibility of FTIR−PAS of IMF of 10 and 1.6 kHz shows twofold deterioration of the signal-to-noise value that supports the choice of the latter IMF for ATR from the viewpoints of the measurement time and sensitivity discussed in the previous sections.

Overall, the absolute increase in the RSD for ATR−FTIR is the same for the whole studied range, which results in relatively small changes in the signal-to-noise ratio (Figure S4, Supporting Information); the most significant difference is in the region of 1900−1340 cm^{-1}, and a slightest, in the region 1350−400 cm^{-1}. However, on the contrary, for some bands in the region of 3000−2500 cm^{-1} and especially for the water band at 1640 cm^{-1}, an improvement in the signal-to-noise ratio was observed with an increase in the fraction size. The latter can result from the ability of smaller particles to adsorb atmospheric water better.

For FTIR−PAS, RSD in the spectra of soil with a particle size of <20 μm ranges between 0.01−0.04 in the regions 3700−2900 and 2000−1350 cm^{-1} and does not exceed 0.2 in the regions 4000−3700, 2900−2000, and 1350−400 cm^{-1}. Thus, the ATR−FTIR reproducibility compared with FTIR−PAS is worse over the entire measurement range. The higher sensitivity of FTIR−PAS in the high wave mid-IR range makes this modality more expedient in hydrogen-bond speciation and CH regions. However, the stably low RSD values in the region of 1350−400 cm^{-1} make it possible to use ATR−FTIR in addition to FTIR−PAS for matrix regions of the soil. These findings confirm the previous data that FTIR−PAS spectra of whole soils

https://doi.org/10.1021/acsomega.1c05702
ACS Omega 2022, 7, 2177−2197

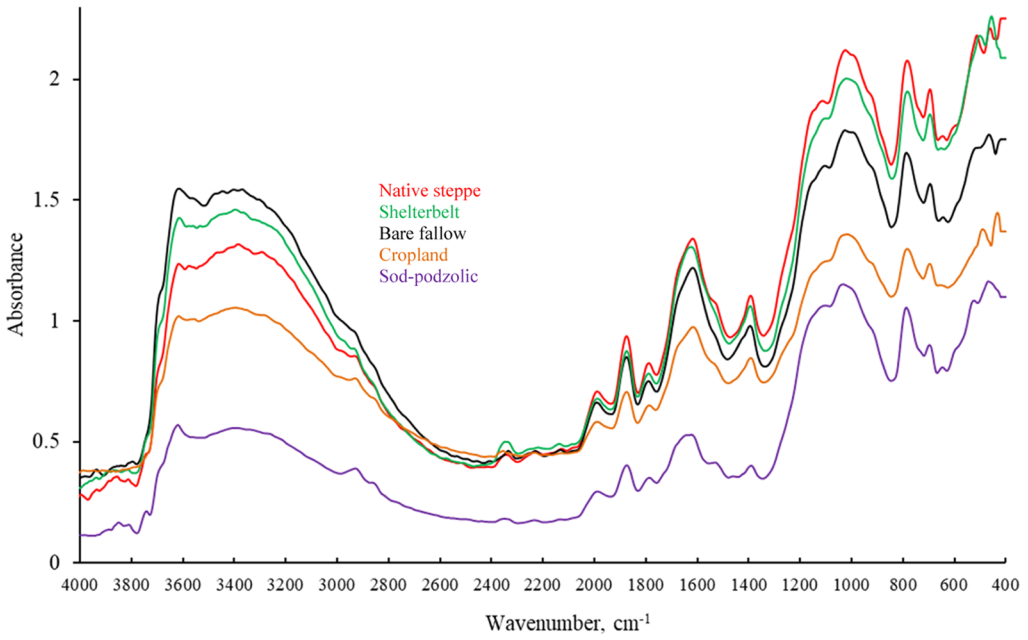

Figure 8. FTIR−PAS spectra (IMF, 1.6 kHz) of soils for a fraction below 20 μm.

of the same type differ from each other less than the ATR−FTIR spectra,[44] but for a more extensive set of samples.

For ATR−FTIR, RSD in the spectra of soil with a particle size of <20 μm is 0.06−0.12 in the regions 3500−2350 and 1200−400 cm^{-1}, and the maximum is 0.4 in the region 4000−3500 cm^{-1}, and more than 0.7 at 2350−1900 cm^{-1}, which provides a good signal-to-noise ratio for all the characteristic bands (Figure S4, Supporting Information). However, for a fraction of 90−100 μm, the reproducibility in the whole mid-IR range is degraded; it is still of 0.08−0.13 and can be considered satisfactory.

3.3. Selection of the Fraction Below 20 μm and Representative Samples. Soil is a heterogeneous, dynamic, and biologically active porous medium whose functions are closely related to its three-dimensional architecture.[5−8] The processes of aggregation and decomposition of aggregates of various hierarchical levels occur dynamically; they depend on many factors, including the intensity of agrogenic effects. Larger aggregates result from the assembly of smaller cemented with various agents: products of soil microflora metabolism, solutions of carbonates, non-silicate minerals of iron and manganese. At the same time, various limits of the physical sizes of particles related to microaggregates are distinguished. They are primarily in the range of 20−250 μm. Some researchers introduce a division into small microaggregates of 20−50 μm and large microaggregates of 50−250 μm. However, particles smaller than 20 or 50 μm are often organized into structural units that include minerals, organic matter(s), and microbial biomass and are thus defined as aggregated.[9] The material of the coarsest fractions is a complex of smaller aggregates collected in a not entirely random order, depending on the origin of the soil and the degree of its variability under the influence of external anthropogenic (agrotechnical) influences.

From the viewpoint of fraction sizes, using the finest soil fractions is preferable to obtain more reliable results and compare them. The reproducibility of the shapes, maximum positions, and integral areas of almost all bands in both methods are higher of the fraction of <20 μm, with the average degradation of the signal-to-noise ratio for both IR modalities ranging from 20 to 140%. Based on error estimations, soil samples require 3−5 replicate measurements. This finding agrees with the improved reproducibility and intensities of bands previously reported by Udvardi et al.[76] and Spitsyn et al.[78]

In this study, average samples of each fraction were taken for each measurement carried out in 10 replicates. Thus, the correspondence of the analytical information of the spectra was ensured by the entire experiment design, from field sampling to spectral information reproducibility during measurements (see the previous section).

Waters and Oades[79] investigated the aggregate fractions of dry sieving <20, 20−53, 53−90 μm, and coarser fractions. They found that the stabilization of the smallest aggregates is associated with the formation of organomineral complexes with a specific humified SOM, in contrast to larger aggregates. SOM of various degrees of humification is present; the smaller, the larger the fraction. Various authors also confirmed the data.[80,81] The differences in microbiological activity (in terms of the content of both the total content of amino sugars and their three types) between the aggregate fractions of <2, 2−20, and 20−250 μm in Mollisol (chernozem analog) fallow soils occupied by herbaceous vegetation and cropland were found.[82] Studies have demonstrated a significant increase in the contents of amino sugars with a decrease in the aggregate size, and it is substantial in the mud fraction, which the authors isolated by sedimentation. They also confirm the differences in the qualitative SOM composition in aggregate fractions.[79] They can also serve as a rationale for choosing a fraction below 20 μm by dry sieving: it contains the most homogeneous in composition and humified SOM reflecting the specificity of the starting material transformation under various conditions of agricultural use.

Narrow-size soil fractions with similar properties facilitate solving the sample representativeness of ATR−FTIR analysis of soil and overall representativeness of IR analysis. Thus, FTIR−PAS was selected for analyzing particles of different shapes and sizes without preparation. In the case of ATR−FTIR, we proceeded from the need to choose the most representative elementary fraction.[9] As the ATR−FTIR crystal area usually does not exceed 3 mm^2, a single soil aggregate with a size of 2−5

https://doi.org/10.1021/acsomega.1c05702
ACS Omega 2022, 7, 2177−2197

Table 5. Comparison of the Area Integrals of Characteristic Bands of Chernozem and Sod-Podzolic Soils by FTIR−PAS

			integral area				
band center, cm^{-1}	high-wave boundary, cm^{-1}	low-wave boundary, cm^{-1}	native steppe	cropland	bare fallow	shelterbelt	sod-podzolic
3693	3704	3683	0.7	1.4	1.8	1.6	1.0
3619	3636	3601	3.3	4.2	4.4	3.9	5.0
2928 and 2847	2946	2831	3.0	2.3	2.8	3.7	3.7
1993	2026	1960	8.6	8.7	11.2	7.5	8.4
1881	1928	1834	40.9	41.6	49.1	36.7	41.7
1794	1830	1758	9.8	10.2	12.3	5.7	9.7
1620	1744	1497	209.0	263.4	275.5	259.5	169.4
1405	1467	1344	28.2	38.6	42.1	35.9	15.6
1111	1141	1082	1.8	3.7	4.6	3.9	4.6
1037	1060	1014	4.2	3.7	4.6	4.5	6.2
989	1010	967	1.6	1.5	2.1	2.1	2.9
780	823	736	44.5	48.4	51.0	48.9	79.0
690	709	672	9.4	9.0	9.5	7.3	10.2
644	663	624	0.7		1.5	0.2	2.3
469	494	444	3.0	2.0	8.6		9.2

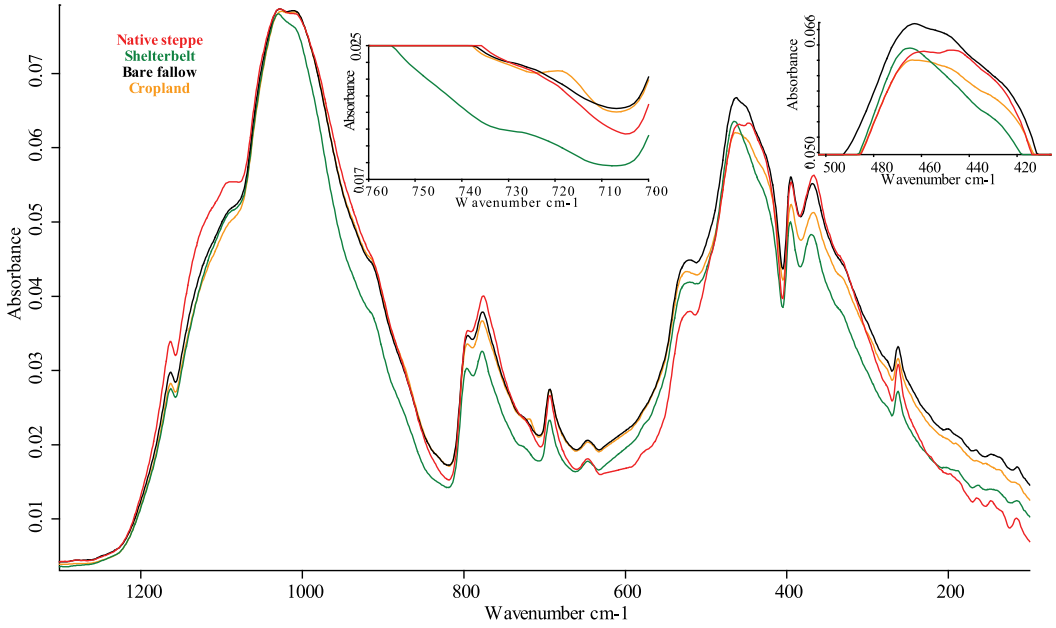

Figure 9. ATR−FTIR spectra of soils for a fraction below 20 μm of chernozem soils.

mm can be placed only, and this cannot be considered representative in any way. Moreover, there is a need to clamp the test object with a screw tightly, and the pressure exceeds 10 t/cm^2 (ca. 98 MPa). Because of this impact, large soil aggregates are often broken down into smaller particles in an uncontrolled manner and may experience mechanochemical changes. In an FTIR−PAS attachment, the sample cup volume is larger, but a soil sample of aggregates larger than 5 mm is also measured with difficulty. Also, the incident IR beam diameter is several millimeters depending on the aperture, limiting the signal-generation zone. Therefore, the smaller the particle size, the larger the number of particles on the ATR−FTIR crystal, and the sample becomes representative. We showed that the fine fraction of <20 μm of both the soils of different types and agricultural use provide the same information as other fractions and whole soils, and it can be a representative sample of the whole soil test object. Thus, it is much more reasonable to use not the whole soil but significantly smaller amounts of fine fractions or, if needed, several narrow-size fractions.

It is possible to further apply this approach with principal component analysis to obtain quantitative results and soil models,[35,40,83] as such models are efficient only when built over representative samples. For example, many protocols and procedures on soil research[16,17] deal with somewhat simplified sample preparation based on drying the soil and removing foreign objects using a sieve size of 2 mm. Unfortunately, such a sample has a too wide size distribution. As the predictive value of models based on large data sets and statistical differences between them depends on the primary data quality, this study shows the way to improve them by studying the fractions, selecting the appropriate size, providing correct information, high sensitivity, and high signal-to-noise ratios for all the characteristic bands.

3.4. Comparison of Soil Types. Different soil types were studied in more detail because the fraction <20 μm provides the best signal-to-noise ratio and reproducibility of all the band maxima's integral areas and positions. FTIR−PAS spectra were recorded with an IMF of 1.6 kHz. Figure 8 shows the shape of

https://doi.org/10.1021/acsomega.1c05702
ACS Omega 2022, 7, 2177−2197

Table 6. Comparison of the Area Integrals of Characteristic Bands of Chernozem and Sod-Podzolic Soils by ATR−FTIR

			integral area				
band center, cm^{-1}	high-wave boundary, cm^{-1}	low-wave boundary, cm^{-1}	native steppe	cropland	bare fallow	shelterbelt	sod-podzolic
3693	3704	3683	0.01	0.05	0.03	0.04	0.04
3619	3636	3601	0.00	0.13	0.11	0.07	0.05
3565	3574	3555	0.02	0.00	0.01	0.01	0.00
2928 and 2847	2946	2831	0.03	0.01	0.00	0.02	0.03
1620	1744	1497	3.30	5.37	4.34	5.07	1.68
1405	1467	1344	0.27	0.56	0.39	0.54	0.13
1165	1176	1154	0.29	0.34	0.32	0.26	0.28
1037	1060	1014	1.03	1.45	1.29	1.34	1.06
989	1010	967	0.76	1.45	1.28	1.29	0.85
780	823	736	8.91	11.40	10.82	9.18	8.64
690	709	672	1.26	1.78	1.61	1.30	1.22
644	663	624	1.50	0.80	0.92	0.93	0.36
450	494	405	19.06	23.16	23.19	22.33	16.83
389	396	383	0.47	0.66	0.66	0.54	0.00
353	367	340	0.63	0.77	0.74	0.43	0.00
321	338	304	0.80	0.88	0.76	0.72	0.00
254	272	235	2.76	2.91	2.93	2.63	0.00

the bands and their integral areas for this method, and this IMF allows recording spectra with a satisfactory signal-to-noise ratio for an adequate time (5−6 min). The integration results were normalized to the integral area of the band of quartz stretching vibrations at 1150 cm^{-1}; see Table 5. The ATR−FTIR spectra after vector normalization are shown in Figure 9. To compare the band integrals, the integration results are normalized to the integral of the band of stretching vibrations of quartz at 1141−1082 cm^{-1}; the results are shown in Table 6.

The band at 3693 cm^{-1} (stretching Si−O−H vibrations) has the largest chernozem cropland and shelterbelt areas. In all spectra, the band at 3620 cm^{-1} is the sharpest for sod-podzolic soil and bare fallow and cropland chernozems and broader in the shelterbelt. This band is naturally present in the fraction of fallows and croplands due to degradation of the clay mineral structure during intensive mechanical soil cultivation.[84,85] It is also worth noting that a small band at 3730 cm^{-1} is the most intense in sod-podzolic soil. FTIR−PAS results are fully coincident, but as stated above, the signal-to-noise ratio for ATR−FTIR is preferable.

Both vector-normalized spectra of CH_2 bands at 2940 and 2860 cm^{-1} and the integration results show that the sod-podzolic soil has the best signal-to-noise values and large areas. It can be related to the dominant (>70%) high-length alkanes in upper horizons of a sod-podzolic soil under broadleaf plant community, the main source of these compounds are epiticular waxes of plant leaf litter.[86] The same can be accounted for the large CH_2 contributions in the native steppe and shelterbelt. The highest total integrals of primary CH_x bands are for the shelterbelt followed by native steppe, while bare fallow is lower, followed by the lowest contents in cropland (Tables 5 and 6). Moreover, in cropland and bare fallow chernozems, the overall shape of this band is different from two other chernozems, and the sod-podzolic sample shows a weak, rather broad band at 2860 cm^{-1} that is the manifestation of methyl groups. Thus, the contribution in the CH region may be from shorter alkane homologues due to the higher biodegradation of alkanes in arable soils. The sod-podzolic soil shows no band at 2860 cm^{-1}. There are no significant differences between FTIR−PAS and ATR−FTIR relative band intensities, although the intensities in the CH region are much more pronounced in FTIR−PAS (Tables 5 and 6).

Significant differences in the spectra of different soil types are in the region 2000−1340 cm^{-1}. The quartz signature bands at 1860 and 1780 cm^{-1} are manifested in the ATR-IR spectra of the sod-podzolic soil only as weak peaks. A broad band at 1700−1550 cm^{-1} also has a different shape in sod-podzolic soil: the band maximum is blueshifted by 10 cm^{-1} compared to chernozems; the 1550 cm^{-1} band (bending −NH− vibrations) has a high intensity.

In FTIR−PAS spectra, the broad band at 1700−1550 cm^{-1} has a different shape compared to ATR−FTIR, with a shoulder band at 1680 cm^{-1}, and a shoulder band at 1530−1520 cm^{-1} appears, which is specific: in cropland and bare fallow, this shoulder is almost absent, while in shelterbelt and native steppe, it is much more pronounced; in sod-podzolic soil, this band is no longer a shoulder, but a sharp band. Moreover, as in ATR−FTIR, sod-podzolic soil has a slightly different shape of the broad band at 1750−1500 cm^{-1}.

The band at 1620 cm^{-1} is well pronounced in both FTIR−PAS and ATR−FTIR spectra, so it can be concluded that it is not due to the quartz overtone bands as they are not well pronounced in ATR modalities. From ATR−FTIR, its area is ca. 1.5-fold larger in chernozems than in the sod-podzolic soil, resulting from the different mechanisms of forming these two contrasting types of soil and the resulting difference in the content of organic matter. Within the studied samples of chernozems, a relatively large area of this band for the cropland soil may be associated with the sampling time at the beginning of the growing season, after the annual application of mineral fertilizers, including ammonia fertilizers that contribute to this band. For this chernozem type, the area is comparable to the area for a shelterbelt, the high content of which of compounds rich in polar functional groups we associate with the seasonal activation of microbiological activity during leaf litter processing.

The bands in the region of 1470−1345 cm^{-1} also differ in chernozems and sod-podzolic soil: the overlapping band maxima are visible in the latter case. Therefore, the normalized integral areas indicate the predominance of SOM in chernozems of the shelterbelt and cropland types, and the normalized integral area of the band at 1620 cm^{-1} in native steppe may

https://doi.org/10.1021/acsomega.1c05702
ACS Omega 2022, 7, 2177−2197

indicate a lower amount of SOM in this chernozem type. Also, sod-podzolic soil has a different band at 1405 cm^{-1}, which applies to stretching −C−O− vibrations.

A higher band intensity at 1405 cm^{-1} (Mg−OH) in chernozems than sod-podzolic soil can be due to the carbonate content of loess-like loams on which chernozems are formed and the absence of carbonates in the sod-podzolic soil. The difference in the band areas of mineral groups is due to lithological features and different mineralogical parent rocks of these two soils.

There are no considerable differences in all five spectra (four chernozems and sod-podzolic) in the matrix II region. The spectra of bare fallow, shelterbelt, and cropland have the most significant similarity. The band at 1165 cm^{-1} appears as a shoulder in the spectra of sod-podzolic soil: in chernozem, this band manifests as a low-intensity sharp peak. However, the largest integral areas of all the identified bands belong to the cropland chernozem. The normalized integration results of this band are also similar. FTIR−PAS gives the same results, although the overall intensity of the band at 1040 cm^{-1} is degraded due to thermal saturation.[87] It also manifests in the signature triplet of quartz overtones at 1980, 1860, and 1780 cm^{-1}. Another difference between FTIR−PAS and ATR−FTIR is the shoulder band appearance at 1350 cm^{-1}, attributed to SOM.

In the matrix I region, all five soil spectra sets are similar. The band at 775 cm^{-1}, bending Al/Mg−O−H vibrations, has the largest normalized integral area for cropland chernozem, as does the band at 697 cm^{-1}. The band at 450 cm^{-1} has the highest relative integral areas in bare-fallow and cropland chernozems. The band at 775 cm^{-1} has the most significant area for sod-podzolic soil, higher than in the chernozems spectra by 65−80%. The quartz matrix bands at 600−400 cm^{-1} are reproduced for all samples. Band positions and relative integral areas by FTIR−PAS differ insignificantly, but overall ATR−FTIR spectra are better resolved and show higher relative intensities, thus differing from FTIR−PAS.

Most differences between the spectra of chernozems and sod-podzolic soils consist in a more explicit manifestation of the bands of stretching CH_2 vibrations at 3000−2800 cm^{-1}. Moreover, there are significant differences at 1760−1340 cm^{-1} related to SOM. The band at 1980 cm^{-1} is the same in all soil types, but in bare fallow, this band integral is 25−35% more than in the other types. The band at 1880 cm^{-1} also has the largest area for the bare fallow, and the difference in the integrals does not exceed 25%. The integration of the band at 1785 cm^{-1} shows a similar dependence. Shelterbelt samples have the smallest integrated areas.

To sum up, sod-podzolic and chernozem soils show distinct differences after fractionation in 1050−950 and 550−300 cm^{-1} governed by the soil matrix. Also, this region shows the differences in spectra of fractions for the same soil type, but various agricultural use and such information cannot be elucidated from the whole soil spectra without fractionation. In the SOM region, the selected fractionation approach and IR modalities provide fewer differences in fraction spectra; and it could be the subject of another study. Indeed, such differences are observed against the background of detector noise, environmental water bands and, as a rule, require significant sample preparation efforts for reliable registration and potential application for analysis. Therefore, more research is needed, specifically designed to assess the prospects for using the detected weak differences.

The differences in the 1900−1340 cm^{-1} region for chernozem soils of different agricultural use most probably related to stretching vibrations of the functional groups of organic matter (−C═C− and −C═O) may indicate that soil material association into aggregates of various hierarchical levels is associated with the organic matter transformation. During agricultural use, depending on the intensity of the agrotechnical load, there is a change in organic matter and mineral components of the aggregates (3775−3000 and 1100−300 cm^{-1}).

3.5. Comparison of FTIR−PAS and ATR−FTIR Modalities for Fractionated Samples. We can compare FTIR−PAS and ATR−FTIR with account for both the sensitivity of measurements and reproducibility of bands. ATR−FTIR results in fewer bands in the SOM region. Also, in terms of reproducibility in the CH and SOM regions, FTIR−PAS has a significant advantage. Stretching CH_x vibrations in the region of 3000−2800 cm^{-1} are observed in most FTIR−PAS spectra, contrary to ATR. In the region of 2100−1520 cm^{-1}, which has many overlapping bands of stretching vibrations −C═C−, −C═O, −C≡N, as well as bending vibrations $-NH_2$, −C═O, −O−H,[56−58] ATR−FTIR is not applicable, while FTIR−PAS demonstrates the best signal-to-noise performance, including a high IMF of 10.0 kHz. At 2500−1200 cm^{-1}, FTIR−PAS allows registering the signature quartz vibrations at 2030, 1950, 1785, 1680, 1504, and 1380 cm^{-1}, which can be used as internal references for quartz-based soils.[38]

To determine the inorganic components of the soil matrix, ATR−FTIR provides higher-intensity modes of the primary vibrations of the quartz matrix, with a favorable signal-to-noise ratio in the region 1350−900 cm^{-1} due to the lack of absorption saturation at the penetration depth of ATR−FTIR, while FTIR−PAS shows a significant change in the relative intensities of the bands at 1170, 1130, and 950 cm^{-1} due to saturation effects.[87] In the quartz lattice region (800−400 cm^{-1}), both FTIR−PAS and ATR−FTIR provide reliable results; however, a lower radiation-penetration depth and radiation intensity in ATR−FTIR may not provide sufficient absorption to reveal all the bands of other matrix minerals. In FTIR−PAS, these bands can still be induced at high IMFs (at a relatively small radiation penetration depth). Thus, FTIR−PAS is better suited for obtaining qualitative and subsequently quantitative information regarding the soil-matrix inorganic components. The method makes it possible to obtain spectra of soil fractions greater than 5 mm without grinding and milling. ATR−FTIR results in high-intensity bands of the soil mineral matrix in its fingerprint region of 1350−900 cm^{-1}; it is advisable to use these methods together as somewhat complementary to each other.

In ATR−FTIR, the penetration depth is limited only by the radiation wavelength and does not exceed 25 μm. Thus, in previous studies on model systems and simpler objects, the possibilities of obtaining additional spectral information with FTIR−PAS varying the penetration depth of radiation were demonstrated both for a decrease (registration of the IR spectra of surface layers) and an increase in the radiation penetration depth.[32,60] However, in this study, the comparison of FTIR−PAS and ATR−FTIR showed no additional information by changing the IMF for neither soil-type fractions nor various agricultural-use chernozem fractions. Although when the fraction size is larger than the penetration depth, only the particle surface generates the signal, thus less information is received. Otherwise, the entire particle generates the photoacoustic signal when the fraction is smaller than the penetration

https://doi.org/10.1021/acsomega.1c05702
ACS Omega 2022, 7, 2177−2197

depth. However, we did not find any significant FTIR−PAS information changes. With a decrease in the IMF, the signal-to-noise ratio improves on average, almost twofold, with an IMF decrease from 1.6 kHz to 150 Hz. However, this multiplies the measurement time of one sample, amounting to hours for a frequency of 150 Hz. Thus, no principal advantages of FTIR−PAS have been found over ATR−FTIR from the viewpoint of information contents. Probably, FTIR−PAS measurement of a signal only from surface groups requires IMFs of hundreds of kHz, which is theoretically possible but requires a special modification of existing commercial PAS attachments and goes far beyond the scope of this study.

Alone or in combination, FTIR−PAS and ATR−FTIR cannot be considered primary methods for the quantitative analysis of SOM components due to the dominance of bands of mineral matrix components in almost the entire IR spectrum of both modalities, which is shown even for chernozems as the soils richest in SOM. Moreover, this is confirmed by the still somewhat similar spectra of chernozems of various agricultural-use types and sod-podzolic soil, containing several times less organic matter and a different structure. Even with the complete removal of organic components, annealing does not change the spectrum significantly.[26] Thus, this casts doubt on the reliability and validity of the existing conclusions on the changes in the SOM structure by IR spectroscopy without chemical separation or speciation.

In general, the considered approach to the analysis of aggregates fractionated by dry sieving with two IR techniques allows a comprehensive assessment of changes in the material composition of soils under the influence of external factors, a highly intense mechanical impact or depletion because of extensive agricultural use (degradation) or restoration of structure and properties when using non-dump and intensive agricultural technologies.

4. MATERIALS AND METHODS

4.1. Instrumentation. IR spectra were recorded on a Bruker Vertex 70 single-beam IR Fourier spectrometer (Bruker Optik GmbH, Germany) equipped with a KBr beam splitter and a wide-range room-temperature DTGS detector or liquid nitrogen-cooled photovoltaic MCT detector. The spectrometer and accessories were continuously purged with −70 °C dew point air (produced by a PG28L Purge Gas Generator, PEAK Scientific, Scotland, UK) with a flow of 500 L/h. The overall laboratory temperature was maintained at 23 °C with an allowable variation of ±1 °C using an air conditioner.

4.1.1. ATR−FTIR. A GladiATR single reflection attenuated total internal reflection accessory with a diamond crystal (Pike Technologies, USA). A background signal was recorded before each new sample. The registration parameters of ATR−FTIR spectra are shown in Table 7. The soil spectra were recorded using a wide-range silicon beam splitter in the range of wavenumbers of 4000−100 cm^{-1}; the baseline was not corrected. Unless otherwise stated, the data were obtained for three replicate measurements; the data were averaged after the whole data post-processing described below (Section 4.2).

4.1.2. FTIR−PAS. An MTEC PAC300 photoacoustic accessory (MTEC Photoacoustic, Inc, USA) was used for direct photoacoustic detection of optical absorption spectra of solids and semisolids with IR Fourier spectrometers. FTIR−PAS spectra were obtained by varying the scanning frequency; software correction of the bands of CO_2 and H_2O was not used. The parameters for recording FTIR−PAS spectra are shown in Table 8. The IR beam from the interferometer is focused to a diameter of 5 mm onto the sample surface. Detector microphone sensitivity is 50 mV/Pa. The sample compartment is purged with helium gas to increase the heat transfer from the sample to the working gas and provide the maximum signal generation.[88] Other details of PAS measurements of soils were selected according to the study.[26]

Samples were placed in a cell installed in the accessory, and the cell compartment was purged with helium for 5−10 s. FTIR−PAS spectra were obtained in continuous-scan modes by varying the IMF (rapid-scan modes of 5.0, 2.5, and 1.6 kHz at the reference He−Ne line of 632.8 nm of the FTIR spectrometer), which correspond to the optical path difference (OPD) velocities of 0.3164, 0.1582, and 0.1012 cm/s, respectively. The number of scans for a sample and background: at an interferometer frequency of 1.6 kHz is 64, at 2.5 kHz, 128, at 5 kHz, 256. In FTIR−PAS mode, the background signal spectrum was recorded using highly pure compressed graphite before each image. Samples weighing 5−10 mg were examined. For IMFs of 1.6 and 2.5 kHz, sample signal amplification modes were 1000 and 2000 times, respectively. The aperture of the FTIR spectrometer was set fully open. In each experiment, the preamplifier gain was set to provide the centerburst interfero-

Table 7. Parameters of Recording Soil Spectra by ATR−FTIR

spectral range, cm^{-1}	4000−100
resolution, cm^{-1}	2
background scan	128
sample scan	128
aperture setting	8 mm
phase resolution	4
phase correction mode	mertz
zero filling factor	1
apodization function	Blackman−Harris 3-Term
sample and background pre-amplification gain	"Ref" (without amplification)
background signal gain	auto
sample signal gain	auto
scanner velocity	10 kHz
detector	room-temperature DLaTGS
source	MIR
beam splitter	KBr
background	diamond crystal with a lowered pressure screw with a flat end

Table 8. Parameters of Recording Soil Spectra by FTIR−PAS

spectral range, cm^{-1}	4000−400
resolution, cm^{-1}	4
background scan	64; 256
sample scan	64; 256
phase resolution	10
phase correction mode	mertz
zero filling factor	2
apodization function	Blackman-Harris 3-Term
aperture setting	8 mm
interferometer frequency	1.6; 5 kHz
sample and background pre-amplification gain	B (middle amplification)
sample signal gain	auto
detector	microphone
source	MIR
beam splitter	KBr

https://doi.org/10.1021/acsomega.1c05702
ACS Omega 2022, 7, 2177−2197

gram amplitude of several volts, without preamplifier clipping, to provide the work of the AD converter of FTIR spectrometers;[88] the gain was set independently for the reference and sample measurements.

The final reference-divided PAS spectrum was automatically calculated by point-by-point division of the single-channel sample spectrum to the single-channel reference spectrum by Bruker OPUS 7.5 software. Software correction of the environmental CO_2 and H_2O peaks was not used during acquisition and applied at this point. The insignificant effect of the water vapor contribution in the region 2000−1200 cm^{-1} was checked by the measurements of the reference material, poly(propylene), and the acquisition of the reference-divided spectra of carbon black against carbon black by the software.[26]

4.2. Data Handling. All spectra were processed in the Bruker OPUS 7.5 software. In the indicated areas, the data were deleted and replaced with a straight line, and the range was chosen as the minimum necessary: 632−590 cm^{-1}, removal of noise caused by strong phonon absorption of the beam splitter; 2350−1865 cm^{-1}, removal of noise caused by strong absorption of the ATR diamond crystal. Smoothing was performed at 13 points, and then extended ATR correction with a refractive index of 1.5 was made. As in all fractions, the silicate matrix content is significant compared to other components, and all spectra were maximized by the band with a maximum at 1007−1032 cm^{-1}. Only smoothing over 25 points and maximization by the band at 1007−1032 cm^{-1} were performed for FTIR PAS.

FTIR−PAS spectra obtained with an interferometer frequency of 1.6 kHz and an amplification of the sample signal of 1000 were smoothed over 25 points, and the intensity was multiplied by $\sqrt{\tilde{\nu}}$.[87] The ATR−FTIR spectra were additionally transformed as follows: $aI_0 + b = I_{corr}$, where I_0 is the intensity of the ATR−FTIR spectra after the operations described above, I_{corr} is the intensity of the ATR−FTIR spectra for comparison with the FTIR−PAS spectra, $a = 150$, $b = 1$.

In FTIR−PAS, the estimation of the radiation penetration depth is made using the dependence of the penetration depth of the heatwave

$$\mu_{PAS}(\tilde{\nu}) = \sqrt{D_T/2\pi V\tilde{\nu}} \quad (1)$$

where D_T is the thermal diffusivity of the sample and V is the interferometer mirror velocity.[87] The OPD velocities of the IR spectrometer were obtained from the IMFs and the He−Ne laser reference line of 632.8 nm: 0.1012 and 0.1582 cm/s, respectively.

The penetration depth of damped IR radiation with the wavenumber $\tilde{\nu}$ into the sample approaching the ATR−FTIR crystal/sample boundary at an angle θ to the normal was estimated as

$$\mu_{ATR}(\tilde{\nu}) = (2\pi\tilde{\nu}n_{ATR}\sqrt{(\sin\theta^2 - (n_{ATR}/n_S)^2)})^{-1} \quad (2)$$

where n_{ATR} and n_S are refractive indexes of the ATR−FTIR crystal and sample, respectively.

4.2.1. Reproducibility. The reproducibility was assessed by recording 10 replicate spectra of chernozem soils of the shelterbelt type for the fraction with a particle size of <20 μm and 10 spectra for the fraction with a particle size of 90−100 μm for the convenience of further comparison of the FTIR−PAS and ATR−FTIR methods with re-registration of the background spectrum after each measurement. After registration, the ATR spectra were not subjected to extended ATR−FTIR correction. Baseline correction and anti-aliasing were not applied. FTIR−PAS spectra were recorded with a complete overfilling of the sample cup and an interferometer frequency of 1.6 kHz. FTIR−PAS spectra were not subjected to automatic baseline correction and smoothing.

RSD and signal-to-noise ratios (S/N = 1/RSD) were calculated as

$$\mathrm{RSD} = \sqrt{\frac{\sum_i (x_i - \bar{x})^2}{n-1}}\,\frac{1}{\bar{x}} \quad (3)$$

4.3. Soil Samples. *4.3.1. Sod-Podzolic Soil.* Samples were taken on the experimental field of the Zelenograd station of V.V. Dokuchaev Soil Institute (village of Eldigino, Moscow region, Russia), operating since 1964. The soil is agrosod-podzolic medium loamy [sod-podzolic, Umbric Albeluvisols Abruptic (WRB 2006), Eutric Podzoluvisols (FAO)] formed on a mantle loam, underlain at a depth of 2−3 m with non-carbonate moraine. Since 2011, the field has not been plowed; a fallow has formed (*Sonchus arvensis*, *Festuca pratensis*, *Phleum pratense*, and *Dactylis glomerata*). Samples were taken in 2016; the coordinates of the sampling site are 56° 07′ 56″ N 37° 48′ 09″ E. Sludge content in the upper (arable) horizon of unflushed full-profile sod-podzolics varies from 10 to 16%.[89] Minerals dominate the mineralogical composition of the clay fraction with a rigid structure (hydromica, kaolinites, chlorites in the upper part). The total mineral content varies along with the profile as 15−18%;[90] organic carbon content, 1.37% w/w; pH 5.96.

4.3.2. Chernozem Soils. Typical chernozems (heavy loamy) of the Kursk region (Russia) with a significantly different history and intensity of agricultural use: native (intact, annually mown) steppe vegetation, permanent bare fallow since 1964, shelterbelt since 1964, arable cropland under wheat, cultivated without crop rotation since 1964.[31] Samples were taken on the territory of the long-term field experiment of the Kursk Research Institute of Agricultural Production and V.V. Alekhin Tsentralno-Chernozemny Nature Reserve of Russia.[91] The granulometric composition of the soil is heavy silty-clay loam. Main components: quartz, 35−40% w/w; illites, 12−15% w/w; smectites, 12−15% w/w; and total organic carbon, 4−6% w/w. The humus horizon (A + AB1) is 105−130 cm. After adding 10% HCl, soil boiling begins at a depth of 65−70 cm. The arable layer bulk density (0−30 cm) ranges from 1.20 to 1.25 g/cm^3.[92]

General soil samples with a mass of 2 kg were taken at the end of May 2017 from sections 1.5 m deep along genetic horizons and additionally with a step of 10 cm. The topsoil layer, 0−10 cm, was taken for this study. General samples were dried for two weeks in air and then stored at room temperature. An average 0.5 kg sample was taken from the corresponding total sample, separated into aggregate fractions by dry sieving (Section 4.3.3 below).

The site of the annually mown native steppe is covered with natural steppe vegetation on V.V. Alekhin Tsentralno-Chernozemny Nature Reserve of Russia; it is a sample of intact typical chernozem. Samples were taken from the section with coordinates 51° 34′ 13.6″ N 36° 05′ 23.1″ E. The vegetation cover is approximately 100% *Bromus riparius* L.,*Festuca sulcata* Hack., *Galium verum* L., *Salvia pratensis* L., *Iris pumila* L., *Adonis vernalis* L., *Vicia tenuifoliaRoth.*, *Stipa pennata*, *Stipa pulcherrima*, and *Stipa tirsa*. Organic carbon content, 5.79% w/w; pH 6.55. Permanent bare fallow since 1964 is a plot bordering on a plot of the annually mown steppe, where the soil is processed annually: plowing without sowing and fertilizers. Thus, since 1964, fresh organic matter almost did not get into this soil type. Soil samples

https://doi.org/10.1021/acsomega.1c05702
ACS Omega 2022, 7, 2177−2197

were taken in the center of the plot, at ca. 50 m from the section on the native steppe sampling site. Organic carbon content, 2.80% w/w; pH 6.0. On the territory of the long-term field experiment of the Kursk Scientific Research Institute of Agricultural Production, soil samples were taken from the protective forest belt (51° 37′ 17.1″ N 36° 15′ 42.0″ E), established in 1964. The forest belt, limiting the experimental fields, forms the soil, the structure of which is restored under the influence of forest vegetation and which, in comparison with the arable chernozem lands, shows a decent structure.[93] Currently, it is a dead-cover forest without a live grass layer, approx. 60 years. Forest-forming species: *Quercus robur*, *Fraxinus excelsio*, and *Acer campestre*. Organic carbon content, 4.75% w/w, pH 6.1. Arable soil is under permanent wheat 51° 37′ 17.1″ N 36° 15′ 42.0″ E with annually applied mineral fertilizers since 1964; organic carbon content, 3.55% w/w; pH 7.3.

4.3.3. Dry Fractionation. Fractionation of the average samples was carried out on an AS 200 sieving machine (Retsch GmbH, Germany) with a dry sieving holder and a set of precision sieves with a stainless-steel mesh, 200 mm in diameter and square mesh sizes of 50, 63, 71, 80, 90, 100, 250, and 500 μm, and 1, 2, and 5 mm (Retsch GmbH). Ultramicro sieves with a diameter of 200 mm and square cells of 20, 30, and 40 μm (Precision Eforming LLC, USA) were used to obtain fine fractions. The dry sieving procedure consisted of sieving the whole sample (ca. 300 g) on a 5000, 2000, 1000, 500, 250, 100, and 50 μm sieve column. Then, a fraction of 50−100 μm (ca. 10−30 g) was processed on a column with 90, 80, 71, and 63 μm sieves. The obtained fraction below 50 μm (ca. 1−20 g) was sieved through a 40, 30, and 20 μm sieve column. The sieving time on each of the three stages was 15 min (paused for a short time each minute) at a sieving amplitude of 3 mm. Thus, soil fractions with particle sizes <20 (<10 and 10−20 for the sod-podzolic soil), 20−30, 30−40, 40−50, 50−63, 63−71, 71−80, 80−90, 90−100, 100−250, 250−500, 500−1000, 1000−2000, 2000−5000, and >5000 μm were obtained. The organic constituents of the fractionated samples were removed by annealing in the air for 3 h at 525 °C in a SNOL 10/900 shaft high-temperature electric laboratory furnace (AB Umega Group, Lithuania).

5. CONCLUSIONS

Thus, dry sieve fractionation of soil samples of different types and agricultural-use conditions into 15 granulometric fractions by dry sieving with sizes from <20 μm to 5 mm was carried out. As far as we are concerned, such detailed fractionation has not yet been used in soil studies using two complementing IR spectroscopy modalities. The analysis of finer fractions improves the signal-to-noise ratio of characteristic IR absorption bands, the reproducibility of the band maximum positions and shape, and an increase in the band intensities, making it possible to recommend such size fractions of soil aggregates for survey and comparison studies. Also, the finest fractions give the most intense signal and readily provide the sample representativeness. Using this approach, we have found small but statistically significant differences between the spectra of different soil aggregate fractions, especially at the macroaggregates level. Thus, studying soil samples with fractionation provides a new information level for soil analysis.

The approach using dry sieve fractionation into relatively small fractions can be applied to other complex heterogeneous objects, but only with the corresponding methodological studies similar to those described in this study. Additional studies are needed, specially designed to assess the prospects of using the detected slight differences. We were limited to dry sieving abilities from the viewpoint of the fraction size range, 20 μm for chernozems and 10 μm for sod-podzolic soils, and the analysis of finer fraction require different approaches like wet sieving and another set of methodological studies. At this research stage, we set the task of studying aggregates that are not exposed to water during the dispersion process; studying the IR characteristics of organic matter depending on the waterproofness of aggregates is the goal of further research.

The differences in fraction spectra must manifest themselves in both FTIR−PAS and ATR−FTIR; thus, these modalities in part confirm and complement each other; thus, their combined use with fractionation is expedient.

■ ASSOCIATED CONTENT

Supporting Information

The Supporting Information is available free of charge at https://pubs.acs.org/doi/10.1021/acsomega.1c05702.

Dependence of the radiation penetration depth in ATR−FTIR spectrometry for quartz and FTIR−PAS spectrometry for chernozem soils; ATR−FTIR spectra of shelterbelt chernozem soil for fractions <20 μm and 90−100 μm for assessing reproducibility; dependence of the RSD on the wavenumber for ATR−FTIR and FTIR−PAS spectra of shelterbelt chernozem soil for fractions below 20 and 90−100 μm; comparison of the averaged signal-to-noise values for the most intense absorption bands for ATR−FTIR and FTIR−PAS spectra of shelterbelt chernozem soil for fractions below 20 and 90−100 μm; and integral areas of ATR−FTIR bands of chernozem and sod-podzolic soils (PDF)

■ AUTHOR INFORMATION

Corresponding Author

Mikhail A. Proskurnin − *Chemistry Department, M.V. Lomonosov Moscow State University, Moscow 119991, Russia;* orcid.org/0000-0001-5577-6883; Email: proskurnin@gmail.com

Authors

Petr K. Krivoshein − *Chemistry Department, M.V. Lomonosov Moscow State University, Moscow 119991, Russia*

Dmitry S. Volkov − *Chemistry Department, M.V. Lomonosov Moscow State University, Moscow 119991, Russia; Department of Chemistry and Physical Chemistry of Soils, V.V. Dokuchaev Soil Science Institute, Moscow 119017, Russia*

Olga B. Rogova − *Department of Chemistry and Physical Chemistry of Soils, V.V. Dokuchaev Soil Science Institute, Moscow 119017, Russia*

Complete contact information is available at: https://pubs.acs.org/10.1021/acsomega.1c05702

Author Contributions

All authors—P.K.K., D.S.V., O.B.R., and M.A.P.—contributed equally.

Funding

This work was supported by the Russian Science Foundation, grant no. 19-13-00117.

Notes

The authors declare no competing financial interest.

■ ACKNOWLEDGMENTS

This research was performed according to the Development program of the Interdisciplinary Scientific and Educational School of Lomonosov Moscow State University, "The future of the planet and global environmental change".

■ REFERENCES

(1) Lal, R. Soil carbon sequestration impacts on global climate change and food security. *Science* **2004**, *304*, 1623−1627.
(2) Imeson, A.*Desertification, Land Degradation and Sustainability*; Wiley, 2012.
(3) Boix-Fayos, C.; Calvo-Cases, A.; Imeson, A. C.; Soriano-Soto, M. D. Influence of soil properties on the aggregation of some Mediterranean soils and the use of aggregate size and stability as land degradation indicators. *Catena* **2001**, *44*, 47−67.
(4) Delelegn, Y. T.; Purahong, W.; Blazevic, A.; Yitaferu, B.; Wubet, T.; Göransson, H.; Godbold, D. L. Changes in land use alter soil quality and aggregate stability in the highlands of northern Ethiopia. *Sci. Rep.* **2017**, *7*, 13602.
(5) Sorour, M. M.; Saleh, M. M.; Mahmoud, R. A. Thermal conductivity and diffusivity of soil. *Int. Commun. Heat Mass Transfer* **1990**, *17*, 189−199.
(6) Bristow, K. L.; Kluitenberg, G. J.; Goding, C. J.; Fitzgerald, T. S. A small multi-needle probe for measuring soil thermal properties, water content and electrical conductivity. *Comput. Electron. Agric.* **2001**, *31*, 265−280.
(7) Jong van Lier, Q. d.; Durigon, A. Soil thermal diffusivity estimated from data of soil temperature and single soil component properties. *Rev. Bras. Cienc. Solo* **2013**, *37*, 106−112.
(8) Józefaciuk, G.; Sławiński, C.; Walczak, R. T.; Bieganowski, A.*Review of Current Problems in Agrophysics*; Institute of Agrophysics PAS, 2005.
(9) Totsche, K. U.; Amelung, W.; Gerzabek, M. H.; Guggenberger, G.; Klumpp, E.; Knief, C.; Lehndorff, E.; Mikutta, R.; Peth, S.; Prechtel, A.; Ray, N.; Kögel-Knabner, I. Microaggregates in soils. *J. Plant Nutr. Soil Sci.* **2018**, *181*, 104−136.
(10) Six, J.; Bossuyt, H.; Degryze, S.; Denef, K. A history of research on the link between (micro)aggregates, soil biota, and soil organic matter dynamics. *Soil Tillage Res.* **2004**, *79*, 7−31.
(11) Filippova, O. I.; Kholodov, V. A.; Safronova, N. A.; Yudina, A. V.; Kulikova, N. A. Particle-Size, Microaggregate-Size, and Aggregate-Size Distributions in Humus Horizons of the Zonal Sequence of Soils in European Russia. *Eurasian Soil Sci.* **2019**, *52*, 300−312.
(12) Kholodov, V. A.; Yaroslavtseva, N. V.; Farkhodov, Y. R.; Belobrov, V. P.; Yudin, S. A.; Aydiev, A. Y.; Lazarev, V. I.; Frid, A. S. Changes in the Ratio of Aggregate Fractions in Humus Horizons of Chernozems in Response to the Type of Their Use. *Eurasian Soil Sci.* **2019**, *52*, 162−170.
(13) Kholodov, V. A.; Yaroslavtseva, N. V.; Yashin, M. A.; Farkhodov, Y. R.; Ilyin, B. S.; Lazarev, V. I. Contents of Organic Carbon and Nitrogen in Particle-Size Fractions of Aggregates of Typical Chernozems (Protocalcic Chernozems). *Eurasian Soil Sci.* **2021**, *54*, 366−371.
(14) Chen, Y.; Zou, C.; Mastalerz, M.; Hu, S.; Gasaway, C.; Tao, X. Applications of Micro-Fourier Transform Infrared Spectroscopy (FTIR) in the Geological Sciences–A Review. *Int. J. Mol. Sci.* **2015**, *16*, 30223−30250.
(15) Falkowski, P.; Scholes, R. J.; Boyle, E.; Canadell, J.; Canfield, D.; Elser, J.; Gruber, N.; Hibbard, K.; Högberg, P.; Linder, S.; Mackenzie, F. T.; Moore, B., 3rd; Pedersen, T.; Rosenthal, Y.; Seitzinger, S.; Smetacek, V.; Steffen, W. The global carbon cycle: a test of our knowledge of earth as a system. *Science* **2000**, *290*, 291−296.
(16) Pansu, M.; Gautheyrou, J.Characterization of Humic Compounds. *Handbook of Soil Analysis*; Springer Berlin Heidelberg: Berlin, Heidelberg, 2006; pp 399−451.
(17) Christensen, B. T.Physical Fractionation of Soil and Organic Matter in Primary Particle Size and Density Separates. In *Soil Restoration*; Stewart, B. A., Ed.; Springer New York: New York, NY, 1992; pp 1−90.
(18) Fultz, L. M.; Moore-Kucera, J.; Calderón, F.; Acosta-Martínez, V. Using Fourier-Transform Mid-Infrared Spectroscopy to Distinguish Soil Organic Matter Composition Dynamics in Aggregate Fractions of Two Agroecosystems. *Soil Sci. Soc. Am. J.* **2014**, *78*, 1940−1948.
(19) Ge, Y.; Thomasson, J. A.; Morgan, C. L. S. Mid-infrared attenuated total reflectance spectroscopy for soil carbon and particle size determination. *Geoderma* **2014**, *213*, 57−63.
(20) Tinti, A.; Tugnoli, V.; Bonora, S.; Francioso, O. Recent applications of vibrational mid-Infrared (IR) spectroscopy for studying soil components: a review. *J. Cent. Eur. Agric.* **2015**, *16*, 1−22.
(21) Raphael, L.Application of FTIR Spectroscopy to Agricultural Soils Analysis. In *Fourier Transforms—New Analytical Approaches and FTIR Strategies*; Nikolic, G., Ed.; InTech, 2011; pp 385−404.
(22) Viscarra Rossel, R. A.; Walvoort, D. J. J.; McBratney, A. B.; Janik, L. J.; Skjemstad, J. O. Visible, near infrared, mid infrared or combined diffuse reflectance spectroscopy for simultaneous assessment of various soil properties. *Geoderma* **2006**, *131*, 59−75.
(23) Volkov, D.; Rogova, O.; Proskurnin, M. Temperature Dependences of IR Spectra of Humic Substances of Brown Coal. *Agronomy* **2021**, *11*, 1822.
(24) Dudek, M.; Kabała, C.; Łabaz, B.; Mituła, P.; Bednik, M.; Medyńska-Juraszek, A. Mid-Infrared Spectroscopy Supports Identification of the Origin of Organic Matter in Soils. *Land* **2021**, *10*, 215.
(25) Ma, F.; Du, C.; Zhang, Y.; Xu, X.; Zhou, J. LIBS and FTIR−ATR spectroscopy studies of mineral−organic associations in saline soil. *Land Degrad. Dev.* **2020**, *32*, 1786−1795.
(26) Krivoshein, P. K.; Volkov, D. S.; Rogova, O. B.; Proskurnin, M. A. FTIR photoacoustic spectroscopy for identification and assessment of soil components: Chernozems and their size fractions. *Photoacoustics* **2020**, *18*, 100162.
(27) Vaudour, E.; Cerovic, Z.; Ebengo, D.; Latouche, G. Predicting Key Agronomic Soil Properties with UV-Vis Fluorescence Measurements Combined with Vis-NIR-SWIR Reflectance Spectroscopy: A Farm-Scale Study in a Mediterranean Viticultural Agroecosystem. *Sensors* **2018**, *18*, 1157.
(28) Margenot, A. J.; Calderón, F. J.; Goyne, K. W.; Mukome, F. N. D.; Parikh, S. J.IR Spectroscopy, Soil Analysis Applications. In *Encyclopedia of Spectroscopy and Spectrometry*; Lindon, J. C., Tranter, G. E., Koppenaal, D. W., Eds.; Academic Press: Oxford, 2017; pp 448−454.
(29) Roy, L.Quantitative FTIR analysis of paraben in finished dosage pharmaceuticals. *Abstracts of Papers of the American Chemical Society*, 2013; Vol. *246*, p 1.
(30) Célino, A.; Gonçalves, O.; Jacquemin, F.; Fréour, S. Qualitative and quantitative assessment of water sorption in natural fibres using ATR-FTIR spectroscopy. *Carbohydr. Polym.* **2014**, *101*, 163−170.
(31) Volkov, D. S.; Rogova, O. B.; Proskurnin, M. A.; Farkhodov, Y. R.; Markeeva, L. B. Thermal stability of organic matter of typical chernozems under different land uses. *Soil Tillage Res.* **2020**, *197*, 104500.
(32) Xing, Z.; Tian, K.; Du, C.; Li, C.; Zhou, J.; Chen, Z. Agricultural soil characterization by FTIR spectroscopy at micrometer scales: Depth profiling by photoacoustic spectroscopy. *Geoderma* **2019**, *335*, 94−103.
(33) Liu, L.; Huan, H.; Zhang, M.; Shao, X.; Zhao, B.; Cui, X.; Zhu, L. Photoacoustic Spectrometric Evaluation of Soil Heavy Metal Contaminants. *IEEE Photonics J.* **2019**, *11*, 1−7.
(34) Ma, F.; Zeng, Y.; Du, C.; Shen, Y.; Ma, H.; Xu, S.; Zhou, J. Soil variability description using Fourier transform mid-infrared photoacoustic spectroscopy coupling with RGB method. *Catena* **2017**, *152*, 190−197.
(35) Ma, F.; Du, C.; Zhou, J.; Shen, Y. Optimized self-adaptive model for assessment of soil organic matter using Fourier transform mid-infrared photoacoustic spectroscopy. *Chemom. Intell. Lab. Syst.* **2017**, *171*, 9−15.
(36) Du, C.; Zhou, J. Evaluation of soil fertility using infrared spectroscopy: a review. *Environ. Chem. Lett.* **2008**, *7*, 97−113.

https://doi.org/10.1021/acsomega.1c05702
ACS Omega 2022, 7, 2177−2197

(37) Huang, P.-M.; Wang, M.-K.; Chiu, C.-Y. Soil mineral−organic matter−microbe interactions: Impacts on biogeochemical processes and biodiversity in soils. *Pedobiologia* **2005**, *49*, 609−635.
(38) Volkov, D. S.; Rogova, O. B.; Proskurnin, M. A. Photoacoustic and photothermal methods in spectroscopy and characterization of soils and soil organic matter. *Photoacoustics* **2020**, *17*, 100151.
(39) Volkov, D.; Rogova, O.; Proskurnin, M. Organic Matter and Mineral Composition of Silicate Soils: FTIR Comparison Study by Photoacoustic, Diffuse Reflectance, and Attenuated Total Reflection Modalities. *Agronomy* **2021**, *11*, 1879.
(40) Du, C.; Zhou, J. Application of Infrared Photoacoustic Spectroscopy in Soil Analysis. *Appl. Spectrosc. Rev.* **2011**, *46*, 405−422.
(41) Lamastra, F. R.; Grilli, M. L.; Leahu, G.; Belardini, A.; Voti, R. L.; Sibilia, C.; Salvatori, D.; Cacciotti, I.; Nanni, F. Diatom frustules decorated with zinc oxide nanoparticles for enhanced optical properties. *Nanotechnology* **2017**, *28*, 375704.
(42) Li Voti, R.; Leahu, G.; Sibilia, C.; Matassa, R.; Familiari, G.; Cerra, S.; Salamone, T. A.; Fratoddi, I. Photoacoustics for listening to metal nanoparticle super-aggregates. *Nanoscale Adv.* **2021**, *3*, 4692−4701.
(43) Changwen, D.; Linker, R.; Shaviv, A. Characterization of soils using photoacoustic mid-infrared spectroscopy. *Appl. Spectrosc.* **2007**, *61*, 1063−1067.
(44) Du, C.; Linker, R.; Shaviv, A. Identification of agricultural Mediterranean soils using mid-infrared photoacoustic spectroscopy. *Geoderma* **2008**, *143*, 85−90.
(45) Du, C.; Zhou, J.; Wang, H.; Chen, X.; Zhu, A.; Zhang, J. Determination of soil properties using Fourier transform mid-infrared photoacoustic spectroscopy. *Vib. Spectrosc.* **2009**, *49*, 32−37.
(46) Woolverton, P.; Dragila, M. I. Characterization of hydrophobic soils: a novel approach using mid-infrared photoacoustic spectroscopy. *Appl. Spectrosc.* **2014**, *68*, 1407−1410.
(47) Linker, R.; Weiner, M.; Shmulevich, I.; Shaviv, A. Nitrate Determination in Soil Pastes using Attenuated Total Reflectance Mid-infrared Spectroscopy: Improved Accuracy via Soil Identification. *Biosyst. Eng.* **2006**, *94*, 111−118.
(48) Linker, R.; Tsror, L. Discrimination of soil-borne fungi using fourier transform infrared attenuated total reflection spectroscopy. *Appl. Spectrosc.* **2008**, *62*, 302−305.
(49) Artz, R. R. E.; Chapman, S. J.; Jean Robertson, A. H.; Potts, J. M.; Laggoun-Défarge, F.; Gogo, S.; Comont, L.; Disnar, J.-R.; Francez, A.-J. FTIR spectroscopy can be used as a screening tool for organic matter quality in regenerating cutover peatlands. *Soil Biol. Biochem.* **2008**, *40*, 515−527.
(50) Artz, R.; Chapman, S.; Campbell, C. Substrate utilisation profiles of microbial communities in peat are depth dependent and correlate with whole soil FTIR profiles. *Soil Biol. Biochem.* **2006**, *38*, 2958−2962.
(51) Fernandes, A. N.; Giovanela, M.; Esteves, V. I.; Sierra, M. M. d. S. Elemental and spectral properties of peat and soil samples and their respective humic substances. *J. Mol. Struct.* **2010**, *971*, 33−38.
(52) Nakamoto, K.; Griffiths, P.Infrared and Raman Spectra of Inorganic and Coordination Compounds. In *Handbook of Vibrational Spectroscopy*; Chalmers, J. M., Ed.; Wiley, 2006.
(53) Jahn, B. R.; Linker, R.; Upadhyaya, S. K.; Shaviv, A.; Slaughter, D. C.; Shmulevich, I. Mid-infrared Spectroscopic Determination of Soil Nitrate Content. *Biosyst. Eng.* **2006**, *94*, 505−515.
(54) Linker, R.; Shmulevich, I.; Kenny, A.; Shaviv, A. Soil identification and chemometrics for direct determination of nitrate in soils using FTIR-ATR mid-infrared spectroscopy. *Chemosphere* **2005**, *61*, 652−658.
(55) Heaney, P. J.; Kronenberg, A. K.; Prewitt, C. T.; Gibbs, G. V.Hydrogen Speciation And Chemical Weakening Of Quartz. *Silica*; De Gruyter, 1994; Chapter 4, pp 123−176.
(56) Xing, Z.; Du, C.; Tian, K.; Ma, F.; Shen, Y.; Zhou, J. Application of FTIR-PAS and Raman spectroscopies for the determination of organic matter in farmland soils. *Talanta* **2016**, *158*, 262−269.
(57) Peltre, C.; Bruun, S.; Du, C.; Thomsen, I. K.; Jensen, L. S. Assessing soil constituents and labile soil organic carbon by mid-infrared photoacoustic spectroscopy. *Soil Biol. Biochem.* **2014**, *77*, 41−50.
(58) Li, S.; Shi, Z.; Chen, S.; Ji, W.; Zhou, L.; Yu, W.; Webster, R. In situ measurements of organic carbon in soil profiles using vis-NIR spectroscopy on the Qinghai-Tibet plateau. *Environ. Sci. Technol.* **2015**, *49*, 4980−4987.
(59) Hofmeister, A. M.; Bowey, J. E. Quantitative Infrared Spectra of Hydrosilicates and Related Minerals. *Mon. Not. R. Astron. Soc.* **2006**, *367*, 577−591.
(60) Du, C.; Goyne, K. W.; Miles, R. J.; Zhou, J. A 1915−2011 microscale record of soil organic matter under wheat cultivation using FTIR-PAS depth-profiling. *Agron. Sustainable Dev.* **2014**, *34*, 803−811.
(61) Changwen, D.; Jing, D.; Jianmin, Z.; Huoyan, W.; Xiaoqin, C. Characterization of Greenhouse Soil Properties Using Mid-infrared Photoacoustic Spectroscopy. *Spectrosc. Lett.* **2011**, *44*, 359−368.
(62) Bock, J.; Su, G.-J. Interpretation of the Infrared Spectra of Fused Silica. *J. Am. Ceram. Soc.* **1970**, *53*, 69−73.
(63) Spitzer, W. G.; Kleinman, D. A. Infrared Lattice Bands of Quartz. *Phys. Rev.* **1961**, *121*, 1324−1335.
(64) Colthup, N. B.; Daly, L. H.; Wiberley, S. E.*Introduction to Infrared and Raman Spectroscopy*; Elsevier Science, 1990.
(65) Inoue, A. Infrared spectra of interstratified illite/smectite from hydrothermally altered tuffs and diagnetic bentonites. *Clay Sci.* **1989**, *7*, 263−275.
(66) Chen, S.; Yin, X.; Wang, S.; Wu, J. Effects of Organic Material Types on Temporal Changes in Characteristics of Humic Acids Extracted from a Chernozem. *Sustainability* **2019**, *11*, 5683.
(67) Wang, S.; Zhang, Z.; Yin, X.; Wang, N.; Chen, D. Influences of Nitrogen Application Levels on Properties of Humic Acids in Chernozem Amended with Different Types of Organic Materials. *Sustainability* **2019**, *11*, 5405.
(68) Lin-Vien, D.; Colthup, N. B.; Fateley, W. G.; Grasselli, J. G.*The Handbook of Infrared and Raman Characteristic Frequencies of Organic Molecules*; Elsevier Science, 1991.
(69) Tatzber, M.; Mutsch, F.; Mentler, A.; Leitgeb, E.; Englisch, M.; Gerzabek, M. H. Determination of organic and inorganic carbon in forest soil samples by mid-infrared spectroscopy and partial least squares regression. *Appl. Spectrosc.* **2010**, *64*, 1167−1175.
(70) Tatzber, M.; Stemmer, M.; Spiegel, H.; Katzlberger, C.; Haberhauer, G.; Gerzabek, M. H. An alternative method to measure carbonate in soils by FT-IR spectroscopy. *Environ. Chem. Lett.* **2006**, *5*, 9−12.
(71) Lilienfein, J.; Qualls, R. G.; Uselman, S. M.; Bridgham, S. D. Soil formation and organic matter accretion in a young andesitic chronosequence at Mt. Shasta, California. *Geoderma* **2003**, *116*, 249−264.
(72) Koike, C.; Noguchi, R.; Chihara, H.; Suto, H.; Ohtaka, O.; Imai, Y.; Matsumoto, T.; Tsuchiyama, A. Infrared Spectra of Silica Polymorphs and the Conditions of Their Formation. *Astrophys. J.* **2013**, *778*, 60.
(73) Proskurnin, M. A.; Korte, D.; Rogova, O. B.; Volkov, D. S.; Franko, M. Photothermal Beam Deflection Spectroscopy for the Determination of Thermal Diffusivity of Soils and Soil Aggregates. *Int. J. Thermophys.* **2018**, *39*, 81.
(74) Branlund, J. M.; Hofmeister, A. M. Thermal diffusivity of quartz to 1,000°C: effects of impurities and the α-β phase transition. *Phys. Chem. Miner.* **2007**, *34*, 581−595.
(75) Yang, C. Q.; Fateley, W. G. The effect of particle size on fourier-transform infrared photoacoustic spectra. *J. Mol. Struct.* **1986**, *146*, 25−39.
(76) Udvardi, B.; Kovács, I. J.; Fancsik, T.; Kónya, P.; Bátori, M.; Stercel, F.; Falus, G.; Szalai, Z. Effects of Particle Size on the Attenuated Total Reflection Spectrum of Minerals. *Appl. Spectrosc.* **2017**, *71*, 1157−1168.
(77) Cantero-Tubilla, B.; Walker, L. P. Transformations to reduce the effect of particle size in mid-infrared spectra of biomass. *Analyst* **2018**, *143*, 5191−5201.
(78) Spitsyn, B. V.; Davidson, J. L.; Gradoboev, M. N.; Galushko, T. B.; Serebryakova, N. V.; Karpukhina, T. A.; Kulakova, I. I.; Melnik, N.

https://doi.org/10.1021/acsomega.1c05702
ACS Omega 2022, 7, 2177−2197

N. Inroad to modification of detonation nanodiamond. *Diamond Relat. Mater.* **2006**, *15*, 296−299.
(79) Waters, A. G.; Oades, J. M.Organic Matter in Water-stable Aggregates. In *Advances in Soil Organic Matter Research*; Wilson, W. S., Ed.; Woodhead Publishing, 2003; pp 163−174.
(80) Puget, P.; Chenu, C.; Balesdent, J. Dynamics of soil organic matter associated with particle-size fractions of water-stable aggregates. *Eur. J. Soil Sci.* **2000**, *51*, 595−605.
(81) Lagomarsino, A.; Grego, S.; Kandeler, E. Soil organic carbon distribution drives microbial activity and functional diversity in particle and aggregate-size fractions. *Pedobiologia* **2012**, *55*, 101−110.
(82) Ding, X.; Qiao, Y.; Filley, T.; Wang, H.; Lü, X.; Zhang, B.; Wang, J. Long-term changes in land use impact the accumulation of microbial residues in the particle-size fractions of a Mollisol. *Biol. Fertil. Soils* **2017**, *53*, 281−286.
(83) Ma, F.; Du, C.; Zhou, J. A Self-Adaptive Model for the Prediction of Soil Organic Matter Using Mid-Infrared Photoacoustic Spectroscopy. *Soil Sci. Soc. Am. J.* **2016**, *80*, 238−246.
(84) Chizhikova, N. P.; Varlamov, E. B.; Savich, V. I. Behavior of Minerals in Agro Soddy Podzolic Soils Resulted from Different Rates of Organic Fertilizers. *Dokuchaev Soil Bull.* **2014**, *76*, 91−110.
(85) Chizhikova, N. P.; Lessovaia, S. N.; Gorbushina, A. A.*Biogenic Weathering of Mineral Substrates (Review)*; Springer International Publishing: ChamCham, 2016; pp 7−14.
(86) Anokhina, N. A.; Demin, V. V.; Zavgorodnyaya, Y. A. Compositions of n-Alkanes and n-Methyl Ketones in Soils of the Forest-Park Zone of Moscow. *Eurasian Soil Sci.* **2018**, *51*, 637−646.
(87) Michaelian, K. H.*Photoacoustic IR Spectroscopy: Instrumentation, Applications and Data Analysis*, 2nd ed.; Wiley-VCH: Weinheim, Germany, 2010; p 402.
(88) McClelland, J. F.; Jones, R. W.; Bajic, S. J.; Griffiths, P. R.Photoacoustic Spectroscopy. In *Handbook of Vibrational Spectroscopy*; Chalmers, J. M., Griffiths, P. R., Eds.; Wiley, 2006.
(89) Sorokina, N. P.; Kozlov, D. N.; Kuznetsova, I. V. Assessment of the postagrogenic transformation of soddy-podzolic soils: Cartographic and analytic support. *Eurasian Soil Sci.* **2013**, *46*, 1007−1019.
(90) Travnikova, L. S.; Artem'eva, Z. S.; Sorokina, N. P. Distribution of the particle-size fractions in soddy-podzolic soils subjected to sheet erosion. *Eurasian Soil Sci.* **2010**, *43*, 459−467.
(91) Cherkassov, G. N.; Masyutenko, N. P.; Gostev, A. V.; Pykhtin, I. G.; Zdorovtsov, I. P.; Akimenko, A. S.Long-Term Field Experiments On Chernozemic Soils Of Kursk Region, Russia. *Soil Organic Matter Dynamics in Long-term Field Experiments and Their Modelling, SSI All-Russia Research Institute of Arable Farming and Soil Erosion Control RAAS: September 14−17, 2010, Kursk: Russia*, 2010; p 35.
(92) Kuznetsova, I. V. Changes in the physical status of the typical and leached chernozems of Kursk oblast within 40 years. *Eurasian Soil Sci.* **2013**, *46*, 393−400.
(93) Khaidapova, D. D.; Chestnova, V. V.; Shein, E. V.; Milanovskii, E. Y. Rheological properties of typical chernozems (Kursk oblast) under different land uses. *Eurasian Soil Sci.* **2016**, *49*, 890−897.

https://doi.org/10.1021/acsomega.1c05702
ACS Omega 2022, 7, 2177−2197